

**LONG TERM PRESENCE OF ISLAND MASS EFFECT AT
TIPUTA CHANNEL, RANGIROA ATOLL**

A THESIS SUBMITTED TO THE GRADUATE DIVISION OF THE UNIVERSITY OF
HAWAI'I AT MĀNOA IN PARTIAL FULFILLMENT OF THE REQUIREMENTS FOR
THE DEGREE OF

MASTER OF SCIENCE

IN

OCEANOGRAPHY

DECEMBER 2019

By Carleigh Vollbrecht

Thesis Committee:

Margaret McManus, Chairperson

Jeffrey Drazen

Jamison Gove

Brian Powell

ACKNOWLEDGEMENTS

I would like to thank my advisor Margaret McManus for the opportunity to explore the data set and for her expertise and guidance throughout this project. I would also like to thank the members of my committee Brian Powell, Jeff Drazen and Jamison Gove for encouraging me to stay the course and keeping me on track. I would also like to thank Paula Moehlenkamp for her assistance with the development of the general linear models and Anna Neuheimer for her analysis of those models. Thanks go to Gordon Walker and Christina Comfort for sharing their field experience. Finally, thank you to my oceanography friends Hyang Yoon and Camilla Tognacchini who added so much joy to the journey.

ABSTRACT

The purpose of this study was to investigate the long term presence of the Island Mass Effect occurring north of Tiputa Channel, Rangiroa Atoll over a 16 year period in relation to environmental influences. Ocean water near Tiputa Channel was compared to open ocean water 46 km to the north. Over a 16 year record, 75.7% of the time, chlorophyll-a in the coastal waters outside Tiputa Channel was higher than 46 km to the north by an average increase in chlorophyll-a of 16%. Primary correlates of the Island Mass Effect at Rangiroa were found to be increased sea surface temperature and decreased photosynthetically available radiation. *In situ* observations in Tiputa Channel over a four day period in April of 2014 were examined to determine the characteristics of the water flowing through the channel. These data shows that water in the lagoon is different having higher temperature, lower salinity, lower density, and higher particulate load compared to ocean water, likely adding the fuel for the localized Island Mass Effect. Understanding forces governing the Island Mass Effect at Rangiroa is important for understanding future changes to ocean productivity brought about by a warming climate and changing environmental conditions.

TABLE OF CONTENTS

ACKNOWLEDGEMENTS.....	i
ABSTRACT.....	ii
LIST OF TABLES.....	iii
LIST OF FIGURES.....	iv
1. INTRODUCTION.....	1
1.1. Rangiroa Atoll.....	1
1.2. Atoll Circulation and Residence Time.....	2
1.3. Atoll Residence Time and Biomass.....	3
1.4. Island Mass Effect.....	4
2. METHODS.....	6
2.1. Study Site.....	6
2.2. Satellite Data.....	8
2.3. Modeled Data.....	10
2.4. Multivariate ENSO Index.....	11
2.5. Instrument Deployment.....	11
2.6. Statistics.....	15
3. RESULTS.....	18
3.1. The Island Mass Effect.....	18
3.2. Correlations.....	24
3.3. Seasonal Patterns.....	28
3.4. <i>In Situ</i> Observations in Tiputa Channel.....	33
3.5. Additional Tests and Data.....	43
4. DISCUSSION.....	46

4.1. The Island Mass Effect	46
4.2. Effects of Physical Forces on IME	48
4.3. How Might Future Changes Affect the IME at Rangiroa?	51
5. CONCLUSIONS.....	52
REFERENCES	53

LIST OF TABLES

Table 1. Latitude and Longitude of MODIS Data.....	8
Table 2. Mooring Deployment Details	15
Table 3. 8-Day Averaged Chlorophyll-a Differences.....	18
Table 4. Measurement of Current Velocity at Moorings A, B and C.....	37
Table 5. Additional Tests and Data.....	45

LIST OF FIGURES

Figure 1. Rangiroa Location Map.....	7
Figure 2. Satellite Map of Study Points.....	9
Figure 3. Bathymetric Tiputa Channel with Moorings A, B, and C.....	12
Figure 4. 8-day Average Chlorophyll-a Difference.....	19
Figure 5. Box Chlorophyll-a Difference by Month.....	20
Figure 6. Monthly Averaged Chlorophyll-a near Tiputa Channel and 46 km Offshore.....	21
Figure 7. Yearly Comparison Chlorophyll-a by Location.....	22
Figure 8. Chlorophyll-a Maps April 2013, 2014, 2015, 2016.....	23
Figure 9. Correlation Coefficient (r-value) Heatmap.....	25
Figure 10. General Additive Model 1: All Predictors.....	26
Figure 11. General Additive Model 2: Best Fit.....	27
Figure 12. Yearly trends Chlorophyll-a Difference and Predictor Variables.....	32
Figure 13. Relative PAR via Voltage Tiputa Channel.....	33
Figure 14. Light Transmittance (%) Tiputa Channel.....	34
Figure 15. Temperature, Salinity, and Density Tiputa Channel.....	36
Figure 16. Horizontal Channel Flow Tiputa Channel.....	38
Figure 17. Vertical Channel Flow Tiputa Channel.....	39
Figure 18. Water Level and Water Flux Tiputa Channel.....	41
Figure 19. Mean Horizontal Current and Wave Power During Ebb Tide.....	41

1. INTRODUCTION

Past research has shown that biological productivity increases around most coral reef islands and atolls across the Pacific basin (Gove et al. 2016). This increase in biological productivity as an island or atoll is approached from open ocean is called Island Mass Effect (IME). A link between physical forces and biological variability has been shown to occur in these systems (Uz et al. 2017). In this paper, I will focus on a single Pacific atoll, Rangiroa, and examine physical forcings as predictors and variability in the biomass of primary producers as the response. Rangiroa was selected for this study because *in situ* data for Tiputa Channel, the main exchange point for water between Rangiroa Lagoon and the ocean, was available. In this thesis, I determine if IME occurs at Rangiroa and then examine what physical forces influence the presence and magnitude of IME. I work with *in situ* data, satellite and modeled data from Rangiroa Atoll in French Polynesia. As our global climate changes, atoll ecosystems are affected by rising ocean temperatures, changes in wave, wind and light fields, as well as rising sea levels, I am interested in how this environmental change will influence atoll systems in the future. Primary production is the basis for the marine food web, understanding the environmental factors that relate to fluctuations in phytoplankton biomass will provide a basis from which one can predict the shifts in the food web that may occur as a result of climate change in this region.

1.1. Rangiroa Atoll

An atoll is a ring-shaped, mostly continuous coral reef enclosing a lagoon located in the ocean (Woodroffe and Biribo 2011). Globally there are 439 atolls, 76 (17.3%) are located in the Tuamotu Archipelago (Goldberg 2016). The Tuamotu Archipelago is a French Polynesian chain of almost 80 islands and atolls in the central South Pacific Ocean. Rangiroa (Tuamotuan for “vast sky”) is the largest atoll in the Tuamotu Archipelago and one of the largest in the world (location Figure 1A and atoll Figure 1B). The atoll perimeter is approximately 200 km consisting of 415 motus or reef islands made of coral and sand surrounding the lagoon. There are two major passes that allow water to flow into and out of the atoll lagoon in the northwest of the atoll. The larger, deeper pass approximately 310 m across is Tiputa Channel, approximately nine kilometers to the west is Avatoru Pass. The southern rim of the atoll is dominated by

“submerged or intertidal areas” (Andréfouët et al. 2001), which allow water from the predominant southern swell to enter Rangiroa’s lagoon. Rangiroa is classified as a partially enclosed atoll.

1.2. Atoll Circulation and Residence Time

In an *enclosed atoll*, an atoll entirely enclosed by land, the primary circulation of the lagoon will be through wave pumping water over the reef rim into the lagoon and the pressure gradient causing advection of water over the rim on the opposing side (Callaghan et. al 2006). This process is modulated by the tide as it raises and lowers the external base water level relative to the atoll rim, increasing or decreasing the amount of water that overflows the rim. In an *open atoll*, an atoll with many passes or low reef allowing the free exchange of water between the lagoon and ocean, the primary mechanism forcing circulation is the tide; the change in lagoon water level will be contained within the tidal range. For a *partially enclosed atoll*, an atoll that is partially enclosed by land acting as a barrier to flow between the lagoon and ocean, like Rangiroa Atoll, the mechanisms forcing circulation are a mix of tidal and wave pumping.

Lagoon residence time is defined by Delessalle and Sournia (1991) as “the average time during which a molecule or unit volume of water stays in a lagoon before being flushed out”.

Andréfouët et al. (2001) calculated the lagoon residence time of twenty Tuamotu Archipelago atolls by looking at the volume of the atoll divided by the volume flux. To calculate the volume flux, the atoll rim was characterized by type and exposure and then assigned an aperture based on measured flows that match those characteristics. This aperture was combined with wave height acquired from satellite altimetry data. During their period of study, wave height was between 1.5 and 3.5 meters and lagoon residence time was between tens of days and several years for the 20 atolls studied. Atoll residence time in Rangiroa Atoll was estimated to be between 130 and 155 days (Andréfouët 2001, Pagès and Andréfouët 2001).

Atolls in the Tuamotu Archipelago exhibit differences in lagoon circulation patterns despite sharing the same general location and climatic conditions. Other forces in addition to waves and tides can drive circulation within an atoll lagoon. Which forcing or set of forces are dominant depends on the morphology of the atoll (i.e., depth, channels, rim type), as well as its location

relative to other atolls. Environmental forces include tidal, wave, wind, solar insolation, and rainfall. Circulation of water in an enclosed atoll with rim above the tidal range would not be affected directly by tides whereas the same atoll with a more open rim or wide passes (partially enclosed atoll), like Rangiroa, would be affected by both tidal and wave forcing. Andréfouët et al. (2001) found that the residence time of water in Rangiroa's lagoon decreased linearly with wave forcing above 1.7 m.

1.3. Atoll Residence Time and Biomass

Water residence time within an atoll lagoon has been recognized to have a strong relationship with phytoplankton biomass (Delesalle and Sournia 1991). If water is flushed too quickly from a lagoon it will be oligotrophic like the surrounding ocean water (Ferrier-Pagès and Furla 2001). Chevalier et al. (2017) found that a water renewal of ~40 days, for Mayotte Lagoon of Mayotte Island, allowed nutrients and organic matter to be recycled multiple times, increasing the biomass in the lagoon before the lagoon water was returned to the open ocean. With Rangiroa's estimated residence time between 130 and 155 days (Andréfouët 2001, Pagès and Andréfouët 2001), nutrients and organic matter are likely recycled multiple times before lagoon water with increased biomass is advected through Tiputa Channel to the coastal ocean.

In addition to the age of the water, the origin of the water and its path of entry to the lagoon is very important to biomass. Water flowing over a reef was found to be different than water flowing through a pass because of the organisms living in the reef change the nutrient content of the water (Chevalier et al. 2017). Reefs trap and recycle nutrients supporting phytoplankton and zooplankton production and growth (Rogers et al. 2017). Chevalier et al. (2017) found that the water exchanges through the passes, like Tiputa Channel, contained higher levels of phytoplankton. Charpy et al. (1997) suggested that phytoplankton biomass inside the lagoon was inversely related to the water exchanged between lagoon and ocean.

Tuamotu atolls have been found to be very productive despite being located in the oligotrophic waters of the South Pacific Subtropical Gyre. Ferrier-Pagès and Furla (2001) looked at two large Tuamotu atolls - Rangiroa and Fakarava Atolls. The investigation found increased biomass in both atoll lagoons compared to the open ocean with differences in the community makeup of

each atoll. In the Tuamotu Archipelago, Charpy et al. (1997) found particulate organic matter to be two to five times higher inside the atolls compared to the open ocean.

For island reefs and atolls, the land can be an important source for nutrients (Dandonneau and Charpy 1985). In the water surrounding Tahiti, increased nutrients were found to occur after rain events caused runoff of nutrient-rich land sediment (Sauzède et. al 2018). Populated islands and atolls may have anthropogenic nutrient inputs such as human waste or agricultural fertilizer (Dandonneau and Charpy 1985).

1.4. Island Mass Effect

Doty and Oguri (1956) tested the hypothesis that the standing crop of plankton increases as an island shore is approached from the open ocean. To test this hypothesis water from four sites on a 60° northeast course between Kaneohe Bay and open ocean were sampled over 14 months. They found that the rate of photosynthetic carbon fixation increased with each site approaching the coast, the site within Kaneohe Bay had the highest rate. The increased standing crop of phytoplankton, termed the Island Mass Effect (IME), was attributed to increased nutrients from the island system.

Further studies have been conducted to investigate the causes of IME. These studies indicate that increased biomass of primary producers is caused by an increase in available nutrients in the euphotic zone near island and atoll systems. Given ample light and nutrients at a favorable temperature, photosynthesis will occur and phytoplankton will grow and multiply, increasing biomass (Kirk 2011). The source of increased nutrients in the euphotic zone can be from one or many the following sources: lagoon flushing, reef nutrient accumulation, nitrogen fixation, terrigenous and anthropogenic runoff, and deep water surrounding the island (Doty and Oguri 1956; Hammer and Hauri 1981; Dandonneau and Charpy 1985; Gove et. al 2016).

Variations in the IME strength have also been observed over both space and time (Dandonneau and Charpy 1985; Charpy et al. 1997; Martinez and Maamaatuaiahutapu 2004; Gove et al. 2016; Sauzède et al. 2018). To examine variations over space, Gove et al. (2016) analyzed chlorophyll-a measurements recorded over ten years via satellite for 24 islands and 11 atolls in the tropical western Pacific. Analysis showed that the primary drivers determining the strength

of the IME were reef area (a larger reef area produced stronger IME), bathymetric slope (a more gradual sloping bathymetry produced stronger IME), geomorphic type (atolls showed stronger IME than islands), and population status (islands and atolls with human population had stronger IME) (Gove et al. 2016).

In the following contribution, I discuss *in situ* data, satellite and modeled data from Rangiroa Atoll, in French Polynesia; investigate if the Island Mass Effect is occurring near Rangiroa's primary pass, Tiputa Channel; give insights into the primary forcing mechanisms of the Island Mass Effect near Tiputa Channel; and suggest how environmental change may influence atoll systems in the Tuamotu Archipelago in the future.

2. METHODS

2.1. Study Site

Rangiroa Atoll is located in the northwestern section of the Tuamotu Archipelago (15.1° S, 147.6° W), about 335 km northeast of Tahiti (Figure 1A). The atoll is the largest in the archipelago, with a lagoon surface area of 1446 km², a maximum depth of 38 m, and an estimated volume of 37.71 km³ (Kumar et al. 2013). The atoll has a saucer shape, its major axis is oriented northwest to southeast and extends for 80 km. Its minor axis is oriented southwest to northeast and extends between 5 and 32 km wide. The atoll perimeter is approximately 200 km consisting of 415 motus or reef islands made of coral and sand surrounding the lagoon. The total land area of Rangiroa is 170 km² (Kumar et al. 2013). Atoll population as of the 2017 census was 2,709 (Institute of Statistics of French Polynesia. 2017).

The lagoon is connected to the open ocean by two large passes in the northwest and approximately 100 small passes in the fringing reef. The Tiputa Channel is a large deep pass located on the upper mid-northwest side of the atoll rim, it is approximately 310 m wide at the narrowest point. Depth along the center axis of Tiputa Channel ranges from approximately 10 m lagoon side to 45 m oceanside with a steep drop off at the mouth to depths below 60 m. Avatoru Pass is a wider, shallower pass located 9 km to the west of Tiputa Channel (Kumar et al. 2013). The southern edge of the atoll is largely fringing reef (Kumar et al. 2013). Andréfouët et al. (2001) classified atoll rims throughout the Tuamotu Archipelago distilling rim types to just nine varieties. Each rim classification indicates a specific amount of permeability between the lagoon and ocean with an accuracy of 85% (Andréfouët et al. 2001). Andréfouët et al. (2001) calculated Rangiroa to have 22% of the perimeter open to the ocean. The porous rim allows both predominant southern and northern swells to add water to the lagoon. Other atolls to the east and west block or alter waves from those directions (Andréfouët et al. 2012).

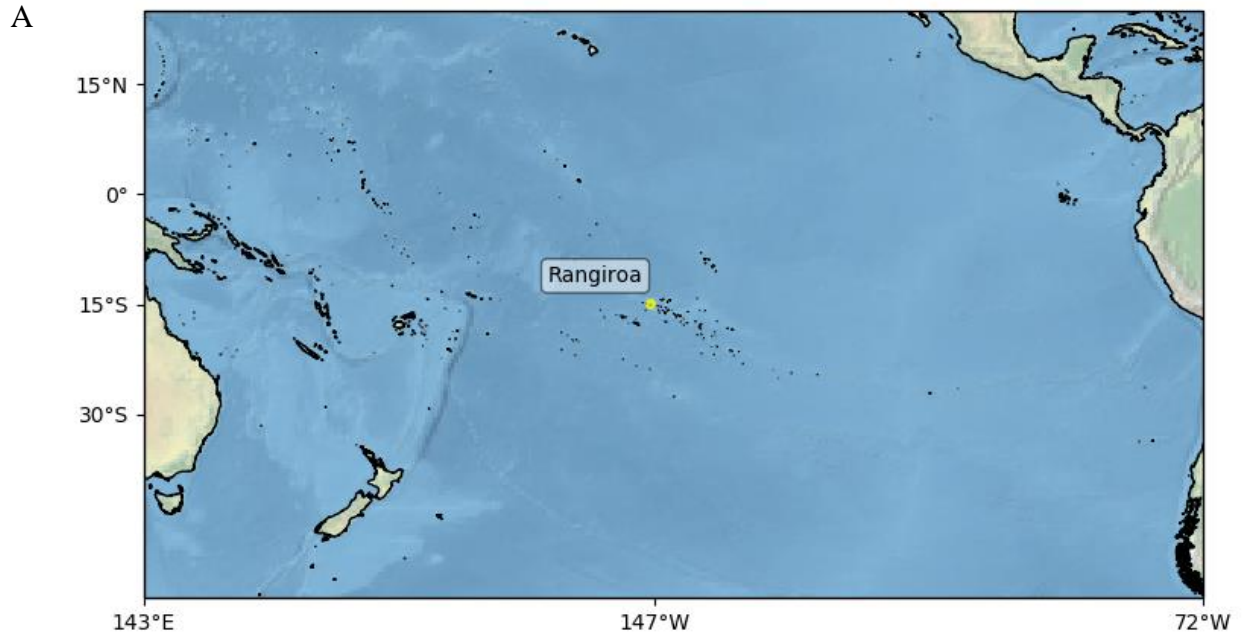


Figure 1A. Southern Pacific Ocean map with Rangiroa marked. 1B. Satellite image of Rangiroa with Tiputa Channel, Avatoru Pass, and the Intergovernmental Oceanographic Commission sea level gauge marked. Image credit: Google Earth.

2.2. Satellite Data

Chlorophyll-a: Chlorophyll-a data is from NASA's Terra and Aqua satellites Moderate Resolution Imaging Spectroradiometer (MODIS) instrument. The 8-day data product is produced by averaging cloud-free daily measurements over an 8-day period over a 4 km square pixel spaced 4.64 km apart. Chlorophyll-a measurements are in mg m^{-3} . The satellite data used in this contribution spans for 16 years from 5 January 2003 to 14 February 2019. Seven MODIS data points (the centers of each pixel) were selected along the northern coast of Rangiroa near Tiputa Channel and Avatoru Pass. These points were selected after filtering for land and shallow water contamination using the 30 m bathymetric contour for the atoll and then further excluding points perpendicular to this contour to eliminate possible contamination by bottom reflectance (after Gove et al. 2016). These seven points near Tiputa Channel were compared to ten points located approximately 46 km directly to the north of Rangiroa Atoll (Figure 2). Taking the difference in average chlorophyll-a concentration between points near Tiputa Channel and points 46 km offshore resulted in 507 sets. Chlorophyll differences less than 0.005 were excluded due to sensor limitations reducing the sets from 507 to 317 for analysis. The latitude and longitude of MODIS data near Tiputa Channel and offshore of Tiputa Channel 46 km to the north are given in Table 1. These points are utilized in both 8-day and monthly comparisons.

Table 1. Latitude and longitude of MODIS data near Tiputa Channel and offshore of Tiputa Channel 46 km to the north. MODIS data is centered at these points.

Latitude/Longitude Tiputa Channel	Latitude/Longitude 46 km Offshore North
1. 14.896° S, 147.729° W	1. 14.479° S, 147.729° W
2. 14.896° S, 147.688° W	2. 14.479° S, 147.688° W
3. 14.896° S, 147.646° W	3. 14.479° S, 147.646° W
4. 14.896° S, 147.604° W	4. 14.479° S, 147.604° W
5. 14.896° S, 147.563° W	5. 14.479° S, 147.563° W
6. 14.938° S, 147.604° W	6. 14.438° S, 147.729° W
7. 14.938° S, 147.563° W	7. 14.438° S, 147.688° W
	8. 14.438° S, 147.646° W
	9. 14.438° S, 147.604° W
	10. 14.438° S, 147.563° W

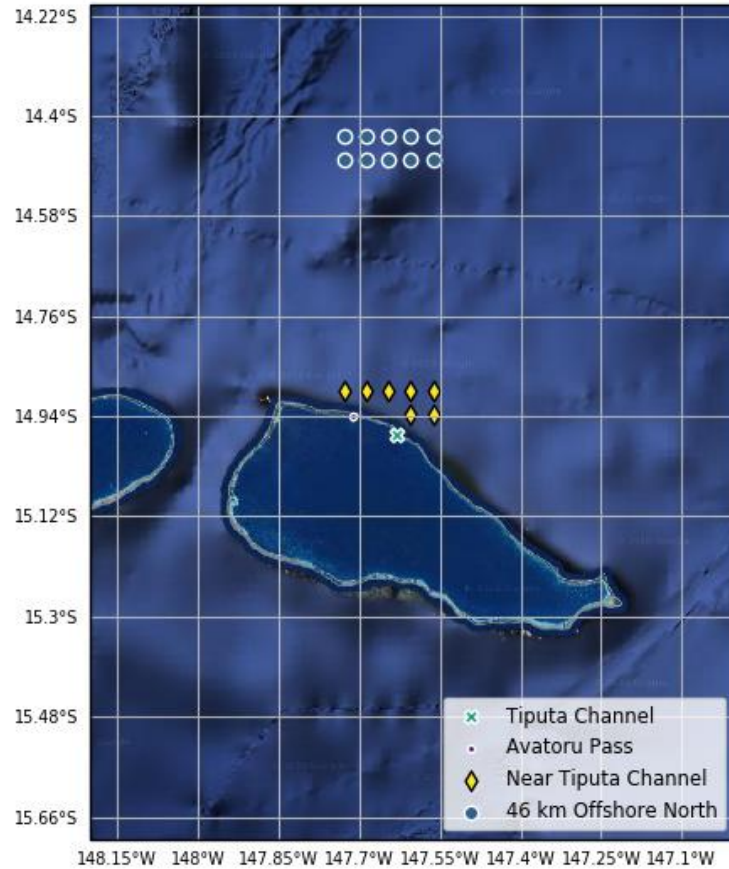


Figure 2. Google satellite map of latitude and longitude of MODIS data near Tiputa Channel and offshore of Tiputa Channel 46 km to the north. Seven points comprising the set near Tiputa Channel are marked with yellow diamonds. Ten points comprising the set 46 km offshore are marked with blue circles. Tiputa Channel is marked with a green 'X' and Avatoru Pass is marked with a small circle.

Temperature: SST ($^{\circ}\text{C}$) measurements are from MODIS, the same source as the chlorophyll-a data. The same seven data point locations near Tiputa Channel were used to calculate a mean SST value for each date-time point. Temperature data were also recorded *in situ* at Mooring C at 37 m depth with a Sea-Bird Electronics 19plus CTD from April 17, 2014 14:54 to April 22, 2014 09:38. Temperature data were recorded every 120 seconds. *In situ* temperature was analyzed to understand the temperature differences of water flowing into and out of the lagoon through Tiputa Channel.

PAR: PAR measurements are sourced the same as SST. The unit for PAR measurements is Einstein $\text{m}^{-2} \text{d}^{-1}$. PAR was analyzed to find the optimal amount required for peak chlorophyll-a. *In situ* relative PAR was also recorded at Mooring C at 37 m depth with a BioSpherical Instruments QSP-2200PD Par Sensor. Relative PAR was recorded every 120 seconds from April 17, 2014 14:54 to April 22, 2014 09:38.

Wind Forcing: Wind direction and magnitude are an 8-day average of daily data. Data are from two sources. From January 1, 2003 to November 20, 2009 the data source is NASA SeaWinds sensor on the QuikSCAT satellite (<https://coastwatch.pfeg.noaa.gov/erddap/griddap/erdQSwind1day.html>), data are 0.125° spaced. Wind data from November 21, 2009 to February 2019 are from the NOAA ASCAT sensor on the METOP satellite (<https://coastwatch.pfeg.noaa.gov/erddap/griddap/erdQAwind1day.html>), data are 0.25° spaced. For each 8-day segment, the mean value of the box bounded by latitudes 14.5° S and 15° S and longitudes 147.25° W 147.5° W was computed. The bounding box is to the east of the chlorophyll-a locations. There is no vertical relief for Rangiroa Atoll or neighboring atolls, so there is no concern about interference from topography. Wind data were time centered and aligned with chlorophyll-a dates.

Rainfall: Daily rainfall totals were downloaded from the multi-satellite Global Precipitation Measurement (GPM) mission, version 5. Data were available in a $0.1^\circ \times 0.1^\circ$ grid, daily rainfall totals are in mm. Area rainfall was downloaded for the period April 18-22, 2014 to correspond with the *in situ* data (<https://pmm.nasa.gov/data-access/downloads/gpm>).

2.3. Modeled Data

Wave Forcing: Wave data were obtained from the WaveWatch III model from two sources. January 2003 to 2013 wave data are from the CAWCR Wave Hindcast 1979-2010 (<https://www.pacificclimatechange.net/document/cawcr-wave-hindcast-1979-2010>) plus the CAWCR wave hindcast extension Jan 2011 - May 2013. Wave data past June 2013 is from the PacIOOS WaveWatch III (WW3) Global Wave Model (http://oos.soest.hawaii.edu/erddap/griddap/NWW3_Global_Best.html). Mean significant wave height, peak wave period, and peak wave direction represent an 8-day average of daily maximum

wave measurements calculated from hourly wave data. Wave data were centered and aligned with chlorophyll-a dates. Wave data were centered south of the atoll at latitude, longitude point 15.5° S, 147.5° W. Mean significant wave height (H_s) and peak period (t_p) were used to calculate wave power (E_f) in kW m⁻¹ using Equation 1 below:

$$E_f = \frac{\rho g^2}{64\pi} H_s^2 t_p / 1000 \quad (1)$$

where ρ is the density of seawater (1024 kg m⁻³) and g is the acceleration of gravity (9.8 m s⁻²). The combination of wave mean significant height and peak period into wave power allows powerful wave events to be identified in a single predictor variable.

2.4. Multivariate ENSO Index

The Multivariate ENSO Index Version 2 (MEI) data are from NOAA (<https://www.esrl.noaa.gov/psd/enso/mei/>). MEI is used to characterize the magnitude of ENSO events, positive MEI values indicate El Niño (warming event) and negative values indicate La Niña (cooling event). MEI data ranges from -2.4 (La Niña) to 2.2 (El Niño). MEI combines oceanic and atmospheric variables into a single index computed 12 times a year in overlapping two-month periods to account for seasonality. The two month seasons consist of Dec-Jan, Jan-Feb, Feb-Mar, Mar-Apr, Apr-May, May-Jun, Jun-Jul, Jul-Aug, Aug-Sep, Sep-Oct, Oct-Nov, and Nov-Dec. Five variables sea level pressure (SLP), sea surface temperature (SST), zonal and meridional components of the surface wind, and outgoing longwave radiation (OLR) over the Pacific region boxed 30°S to 30°N and 100°E to 70°W have their variances normalized and are then combined to compute the MEI. Rangiroa Atoll is located within the bounding box used to calculate MEI.

2.5. Instrument Deployment

Four Sontek Acoustic Doppler Profilers (ADPs) were deployed along the main axis of Tiputa Channel to assess the spatial and temporal variability in ocean currents (Figure 3). From earlier work (Kruger 2013), it was evident that currents flow predominantly along the axis of the channel (i.e., there is little to no cross channel flow). Prior to deploying instrumentation in Tiputa

Channel, all ADPs were compass calibrated, bench tested and field tested in their respective mooring frames. The four ADPs were tested, each collecting between one and two hours of data during the test deployments. These data were quality controlled and reviewed for errors. No sensor exhibited erroneous data during test deployments.

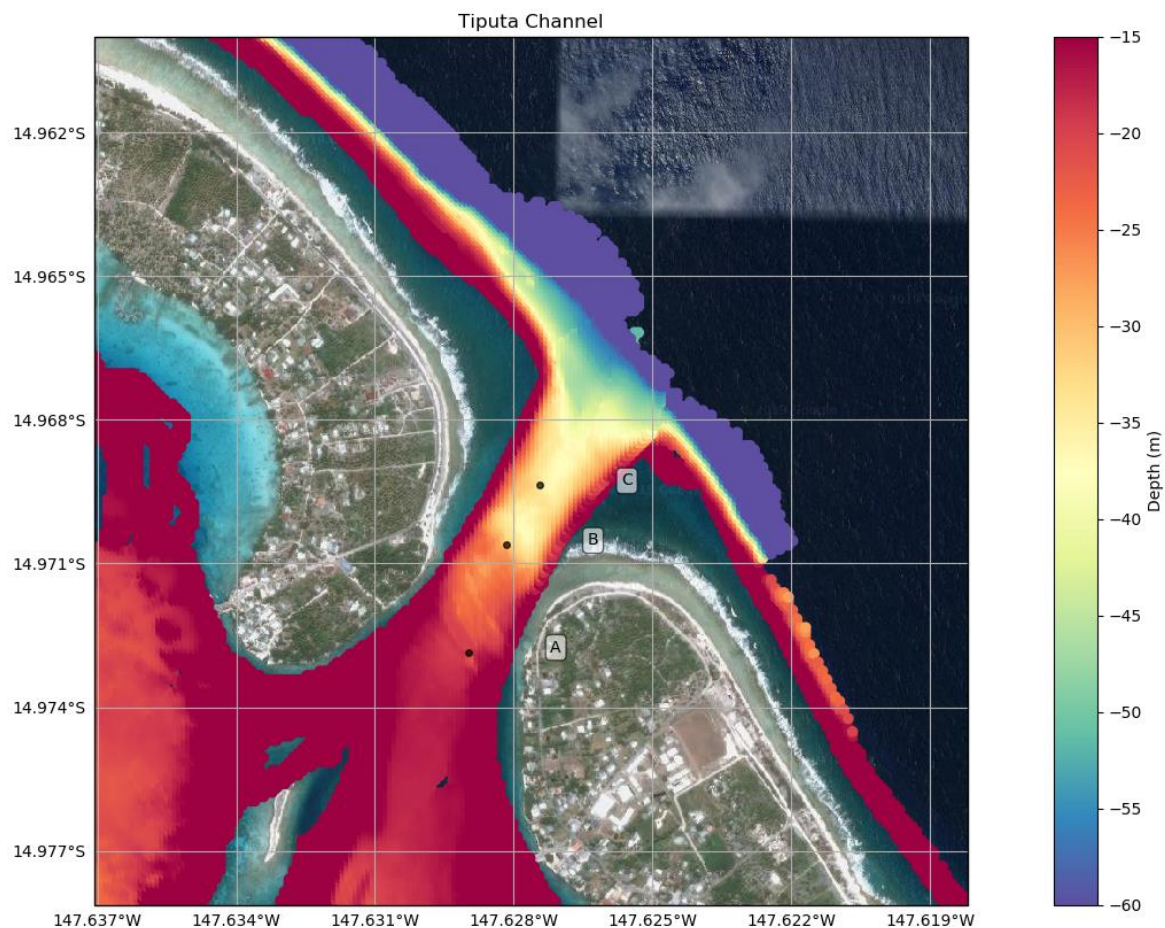


Figure 3. Bathymetric data from Tiputa Channel collected by the Secretariat of the Pacific Community Applied Geoscience Division (SOPAC) overlaid on a Google satellite image. Bathymetric data are indicated by color with red being shallower and blue being deeper. Deployment locations of three moorings are marked A, B, and C. See Table 2 for mooring details.

Oceanographic moorings deployed along the primary axis of the channel were placed in consecutively deeper locations from the lagoon to the ocean. Three moorings (Moorings A, B, and C at 22.5, 29.5 and 38 m, respectively) were deployed via SCUBA divers using lift bags, enabling a controlled descent and ensuring precise instrument placement on the seafloor. Moorings A–C, SonTek (SonTek: www.sontek.com) 1000 kHz ADPs, were all configured in the

same manner; with an upward-looking Sontek ADP mounted in a gimbaled aluminum tripod frame. Each mooring, once firmly placed on the seafloor, was leveled using a small, hand-held level and secured in the gimbal. Moorings A–C sampled at 1 m depth bins averaged over 30 sec every 120 sec (Table 2). The fourth mooring was placed using floats at 58 m depth, data for this mooring is not shown because it was moved by the strong channel current after placement despite being weighted with two concrete blocks weighing between 181.4 and 204.2 kg.

The currents in Tiputa Channel are known to be very strong. Due to the strong currents, the in-water mooring weight for each sensor was increased above the weight normally used in routine oceanographic deployments. Additionally, because of bottom bathymetry, Mooring A was deployed in an approximately 3.5 m deep groove that runs perpendicular to the axis of Tiputa Channel. Currents in the groove are minimal, which ensured the stability of the mooring. Thus, only depth bins above the height of the groove (3.5 m) are presented for Mooring A.

The magnetic declination for 14.97° S 147.63° W in April of 2014 was 12.2° E changing by 0.02° E per year (<http://www.ngdc.noaa.gov/geomag-web/>). Thus, to convert a magnetic bearing to a true bearing (i.e., one that you could plot on a map) one adds the magnetic declination. The declination of the location of the oceanographic study is 12.2° E (+12.2°). The magnetic declination was added during post-processing.

Data availability for Moorings A–C is based on the time periods in which the moorings were retrieved and recovered (cf. Table 2). Deployment and retrievals were principally dictated by the availability of suitable SCUBA diving conditions within the targeted study time frame. Due to high current velocities, there is only a short period of time between ebbing and flooding tides, during which it was safe to deploy and recover instrumentation.

Additional sensors were deployed on Mooring C (38 m) to assess water conditions. A Sea-Bird Electronics 19plus CTD (<http://www.seabird.com>) measured conductivity (from which salinity can be calculated), temperature, and pressure (from which water level can be calculated). A Wet Labs C-Star transmissometer (<http://www.wetlabs.com>) measured light transmittance (a proxy for water clarity). A BioSpherical Instruments QSP-2200PD PAR Sensor

(<http://www.biospherical.com>) measured photosynthetically active radiation (PAR) (light levels). The QSP-2200PD PAR sensor series require a log amplifier in order to convert the raw voltage output into units of irradiance. The Sea-Bird Electronics 19plus used in the deployment was not equipped with a log amplifier, thus absolute irradiance information was not possible to attain. However, the raw voltages may still be used to demonstrate relative levels of irradiance. The sensor captures light wavelengths between 400 and 700 nm, the spectrum used by plants for photosynthesis (Biospherical Instruments Inc. 2007). Data were sampled every two minutes. The Sea-Bird Electronics 19plus CTD was calibrated at the Sea-Bird factory. The C-Star transmissometer was calibrated in the laboratory post-deployment according to the information found in Sea-Bird electronics Application Note 7.

All data were collected and downloaded in Universal Time Coordinated (UTC) and converted to local time for presentation in this thesis (-10 hours UTC). Details for each deployment including mooring deployment set up, mooring depth, duration of deployment and other pertinent information are listed in Table 2.

Table 2. Information for each mooring deployed as part of the oceanographic study of Tiputa Channel that occurred between 17 and 23 April 2014. See Figure 3 for mooring locations.

	Mooring A	Mooring B	Mooring C
Manufacturer	Sontek	Sontek	Sontek
Frequency (kHz)	1000	1000	1000
Latitude (°S)	14.9729	14.9706	14.9694
Longitude (°W)	147.6290	147.6282	147.6274
Depth: Sea Floor (m)	22.5	29.5	38.0
Depth: ADP Transducer (m)	21.5	28.5	37
Bottom Bin data (m from surface)	16.5	26.5	36.0
Top Bin (m from surface)*	4.5	4.5	13.0
Orientation of Sensor	Up	Up	Up
Principle Axis of Flow (°) (true)	32.2/212.2°	32.2/212.2°	32.2/212.2°
Cell size (m)	1	1	1
Blanking Distance (m)	1	1	1
Average Interval (s)***	30	30	30
Sampling Interval (s)**	120	120	120
Current Measurement Units	cm s ⁻¹	cm s ⁻¹	cm s ⁻¹
Start Time	4/19/2014 06:52	4/19/2014 16:28	4/17/2014 14:54
End Time	4/22/2014 11:28	4/22/2014 09:50	4/22/2014 09:38

*The upper limit of measurable current data is dictated by both the frequency of the instrument (high frequencies attenuate more quickly), as well as the amount of scattering particles in the water column. Therefore, there were periods where data collected do not reach this upper limit.

**Average Interval represents the time period over which the instrument is averaging during data collection.

***Sampling Interval is the time period, or interval, between data collection.

2.6. Statistics

Mann-Whitney U Test: The Mann-Whitney U Test is a nonparametric test used to indicate the probability that two independent samples are from the same distribution, in other words, this test is used to check the likelihood that two sets of measurements are different sets rather than belonging to one larger set. To perform the test (1) order all measurements by magnitude and assign rank, and (2) average the ranks for each set. (3) If the mean of the ranks is very different the p-value will be low (Spiegel and Stephens 2011). This test was performed using R (R Core Team 2019) to check the probability that chlorophyll-a concentrations near Tiputa Channel and 46 km offshore to the north were from sets with different distributions.

Pearson's Pairwise Correlation: Pearson's method was used to test for a linear relationship between two sets of data. Equation 2 below calculates the correlation coefficient or r-value (r) using each sample point (i) in the two datasets (x and y)

$$r = \frac{\sum(x - m_x)(y - m_y)}{\sqrt{\sum(x - m_x)^2} \sqrt{\sum(y - m_y)^2}} \quad (2)$$

where m_x is the mean of the set x and m_y is the mean of the set y . R-values have a sign and magnitude. Positive signs indicate a positive correlation, negative signs indicate a negative correlation. The magnitude spans from 0 to 1 with larger numbers showing a higher correlation. The p-value indicates the probability that the r-value relationship is not true. The p-values span from 0 to 1 with results less than 0.05 indicating significance (Abbott 2017).

General Additive Model (GAM): A general additive model was used to investigate nonlinearity in the relationship of the response of chlorophyll-a difference between near Tiputa Channel and 46 km offshore to the predictor variables (sea surface temperature (SST), photosynthetically available radiation (PAR), wind magnitude, wind direction, wave power, wave direction, and the multivariate ENSO index (MEI)). The response and predictors are time aligned (no lag), entries missing a value were removed from the dataset, resulting in 310 sets. To deal with temporal autocorrelation, a variable (SampleDay) containing the number of days since the first sample was added to each set. Each of the predictor variables was added to the equation as a non-parametrically smoothed function. Wind magnitude and direction are assessed together (as a non-parametrically smoothed function), allowing magnitude to be smoothed using thin plate regression spline and direction to be accessed with cyclic cubic regression splines. Wave power and direction are treated the same as wind magnitude and direction. The basis for smoothing of SST, PAR, MEI, and SampleDay is thin plate regression spline. Model (Equation 3) was run in R using package mgcv, model family Gaussian with identity linking function.

$$g \{E(y_i)\} = f_1(SST_i) + f_2(PAR_i) + f_3(WindMagnitude_i, WindDirection_i) + f_4(WavePower_i, WaveDirection_i) + f_5(MEI_i) + f_6(SampleDay_i) \quad (3)$$

The general additive model run returned 128 models representing all possible combinations of the predictors. The best fit model (Equation 4) weighted at 0.149 and excludes wave power, wave direction, and MEI parameters.

$$g \{E(y_i)\} = f_1(SST_i) + f_2(PAR_i) + f_3(WindMagnitude_i, WindDirection_i) + f_4(SampleDay_i) \quad (4)$$

3. RESULTS

3.1. The Island Mass Effect

To test for the presence of Island Mass Effect (IME), 8-day averaged chlorophyll-a data were examined. To compare the set of points at near Tiputa Channel to the set of points at 46 km offshore to the north (c.f. Figure 2), the difference was taken of each set. Over a period of 16 years, from January 2003 to February 2019 chlorophyll-a was higher near Tiptua Channel compared to offshore waters 75.7% of the time (Table 3). The Island Mass Effect (IME) is clearly present in coastal waters offshore of Tiputa Channel.

Table 3. The number of 8-day averaged chlorophyll-a data sets where a comparison between the area directly offshore Tiputa Channel and the area 46 km to the north were possible. The number of data sets where the 8-day averaged chlorophyll-a was higher directly offshore Tiputa Channel (chl_diff positive), and lower directly offshore Tiputa Channel (chl_diff negative).

	Number of records	% of the total	Mean of values
chl_diff records	317	100%	0.008
chl_diff positive	240	75.7%	0.015
chl_diff negative	77	24.3%	-0.013

Recorded values over the 16-year study period for chlorophyll-a difference range from -0.043 to 0.091 mg m⁻³ with a mean value of 0.008 mg m⁻³. The mean positive chlorophyll-a difference was 0.015 mg m⁻³ and the mean negative chlorophyll-a difference was -0.013 mg m⁻³ (Figure 4). Chlorophyll-a difference varies greatly year to year. Seasonal trends in chlorophyll-a difference are not strong or consistent across all years. The lowest value -0.043 mg m⁻³ was recorded in September 2012, the highest value 0.091 mg m⁻³ was recorded in March 2010 (Figure 4).

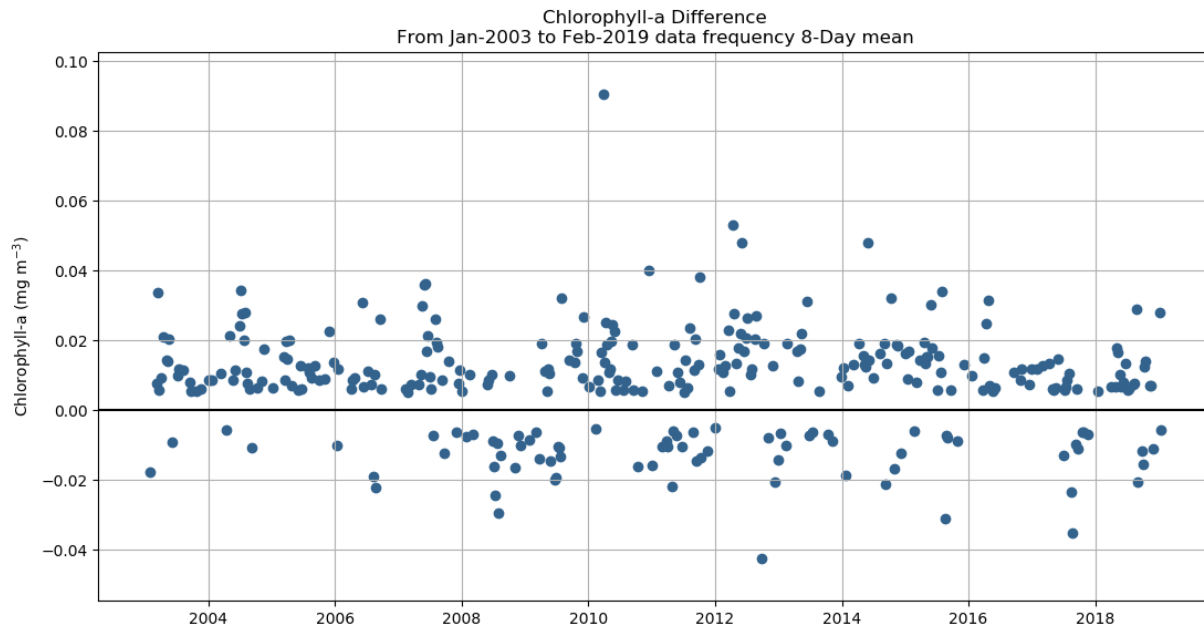


Figure 4. Difference between 8-day average chlorophyll-a data between near Tiputa Channel and 46 km offshore from January 2003 to February 2019. Positive values represent times when the IME was present, negative values represent times when the IME was not present.

The chlorophyll-a difference between near Tiputa Channel and 46 km offshore by month, between January 2003 and February 2019 are presented in Figure 5. The month with the highest chlorophyll-a difference across the 16-year time span is May with a mean chlorophyll-a difference of 0.014 mg m^{-3} . The month with the lowest chlorophyll-a difference across the 16-year time span is September with a mean chlorophyll-a difference of 0.002 mg m^{-3} . March has the highest variability with the standard deviation of 0.020 mg m^{-3} and February has the lowest variability with the standard deviation of 0.009 mg m^{-3} . Data are spaced unevenly throughout the year due to clouds during the rainy summer season. This results in fewer chlorophyll-a records in the months of October through March.

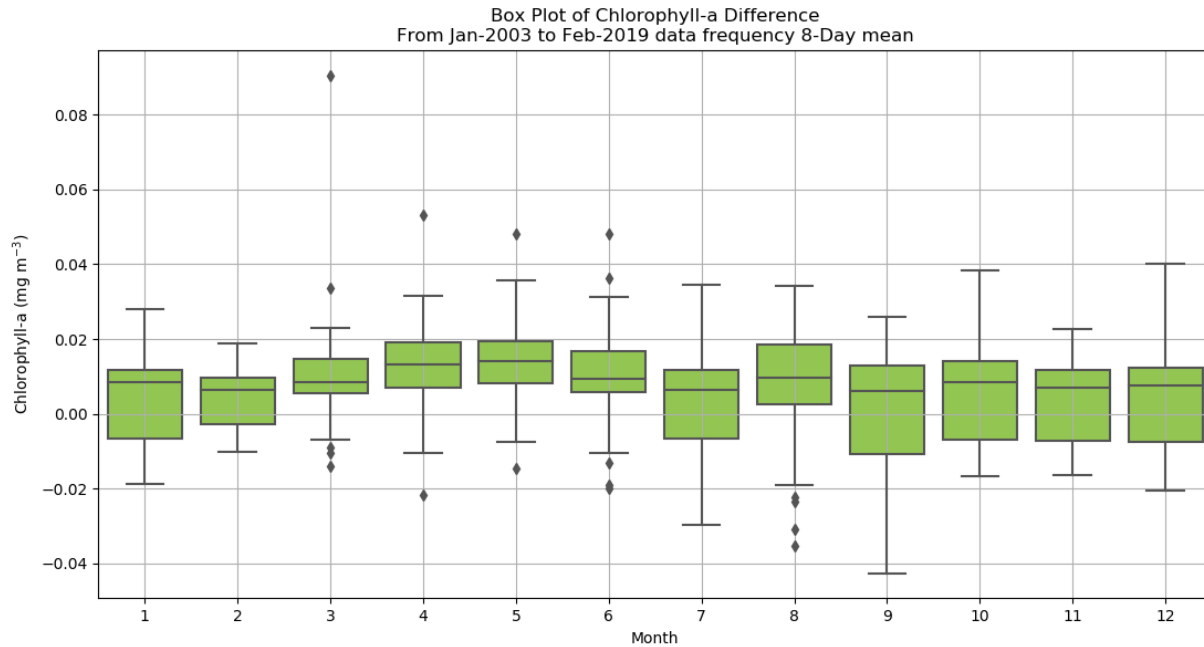


Figure 5. Box plot of 8-day average chlorophyll-a difference between near Tiputa Channel and 46 km offshore by month, derived from data between January 2003 and February 2019. The central mark in each box is the median, the bottom and top edges of the box are the 25th and 75th percentiles. Diamonds indicate outliers.

Chlorophyll-a data from near Tiputa Channel and 46 km offshore plotted over the 16 year study period were used to view long term chlorophyll-a trends at each location (Figure 6). Across the 16 year time period, the 8-day averaged chlorophyll-a data near Tiputa Channel ranged from 0.026 to 0.160 mg m^{-3} with a mean value of 0.072 mg m^{-3} . Chlorophyll-a concentration 46 km offshore ranged from 0.025 to 0.148 mg m^{-3} with a mean value of 0.067 mg m^{-3} . Chlorophyll-a near Tiputa Channel and 46 km offshore follow similar, though not identical, patterns of both increases and decreases through the record. A Mann-Whitney U Test applied to the two locations was significant ($W=58995$, $p\text{-value} < 0.05$), indicating that chlorophyll-a concentrations from Tiputa Channel are from a different distribution than chlorophyll-a concentrations 46 km offshore. Over the 16 year period, averaged chlorophyll-a concentration at Tiputa Channel is 16% greater than the concentration 46 km offshore to the north.

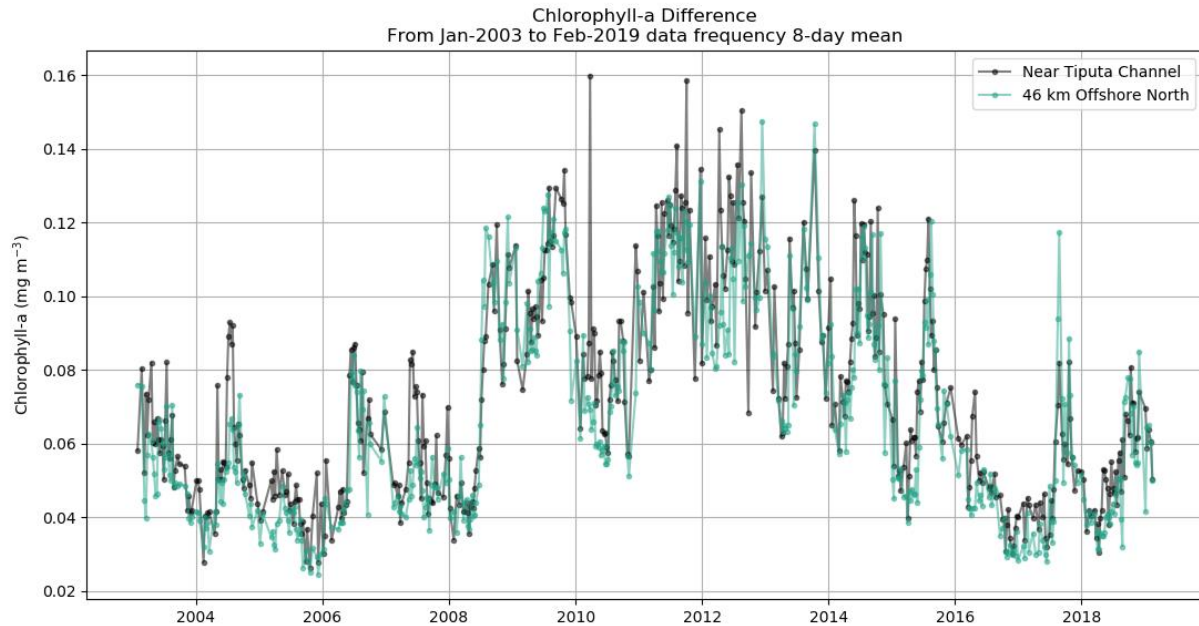
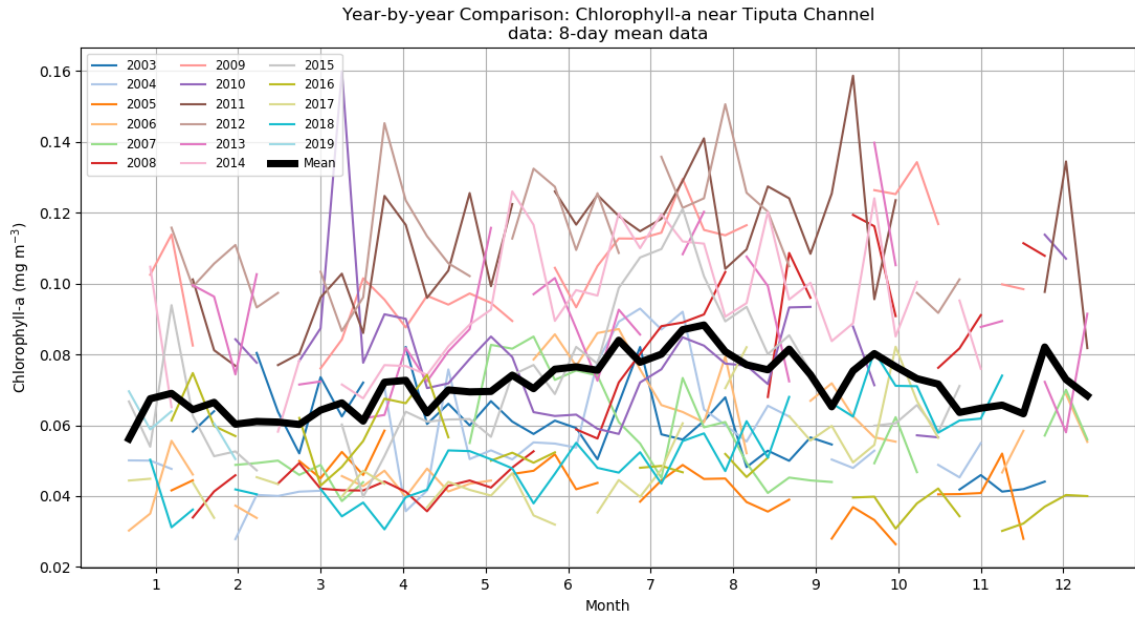


Figure 6. Chlorophyll-a data near Tiputa Channel (dark blue) and 46 km offshore (aqua) data is 8-day average. Timespan is between January 2003 and February 2019.

Chlorophyll-a near Tiputa Channel and 46 km offshore both show a gradual rise in chlorophyll-a from March through August when all years are averaged, however when comparing year to year, this pattern is not consistent and there is wide variability across the years for each month (c.f. Figure 5, Figure 6, Figure 7).

Monthly chlorophyll-a product was mapped (Figure 8) with the land and lagoon masked. Mean chlorophyll-a concentration for April can be visualized across four consecutive years (2013, 2014, 2015 and 2016). Although the chlorophyll-a concentrations fluctuate from year to year, higher concentration of chlorophyll-a can be seen near Tiputa Channel compared to the open ocean directly north in each year. April 2016 chlorophyll-a near Tiputa Channel was 0.068 mg m^{-3} compared to 0.043 mg m^{-3} 46 km offshore, difference of 0.025 mg m^{-3} . Chlorophyll-a concentration differences were lower for example at 0.005 mg m^{-3} in 2013, 0.005 mg m^{-3} in 2014, and 0.008 mg m^{-3} in 2015. Although the chlorophyll-a concentration differences in 2013, 2014 and 2015 were lower than 2016, they were all positive, which means that the coastal waters outside Tiputa Channel had higher chlorophyll-a than 46 km offshore.

A



B

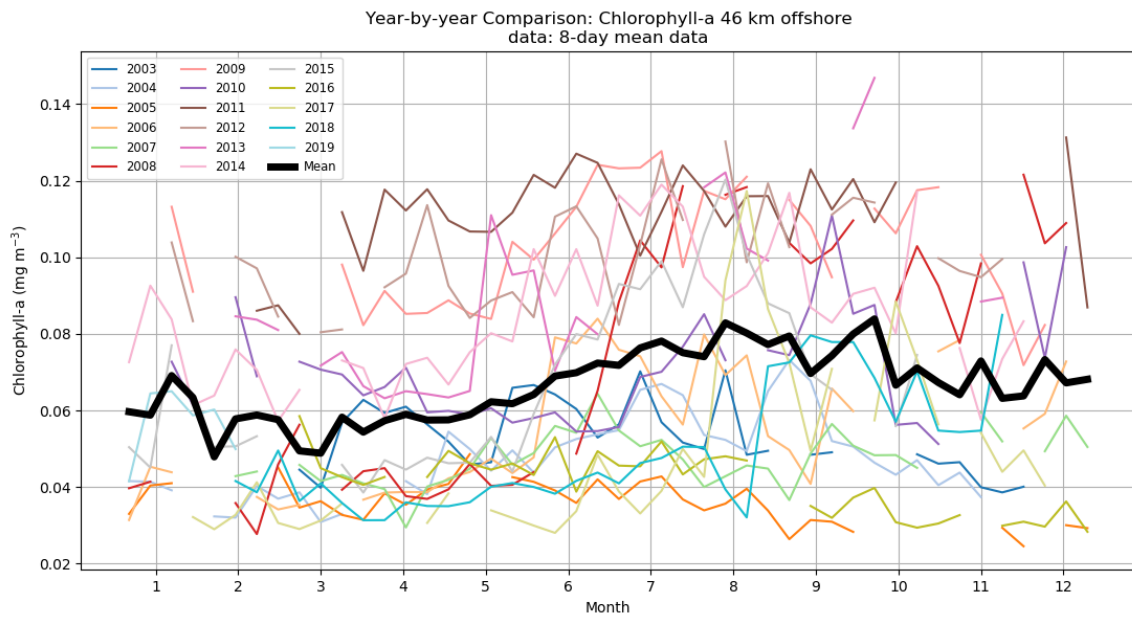


Figure 7A. Yearly comparison of 8-day mean chlorophyll-a concentration (mg m^{-3}) near Tiputa Channel. See key in figure for color reference. The dark black line is the collective 8-day mean. 7B: Same as 7A, but for 46 km offshore.

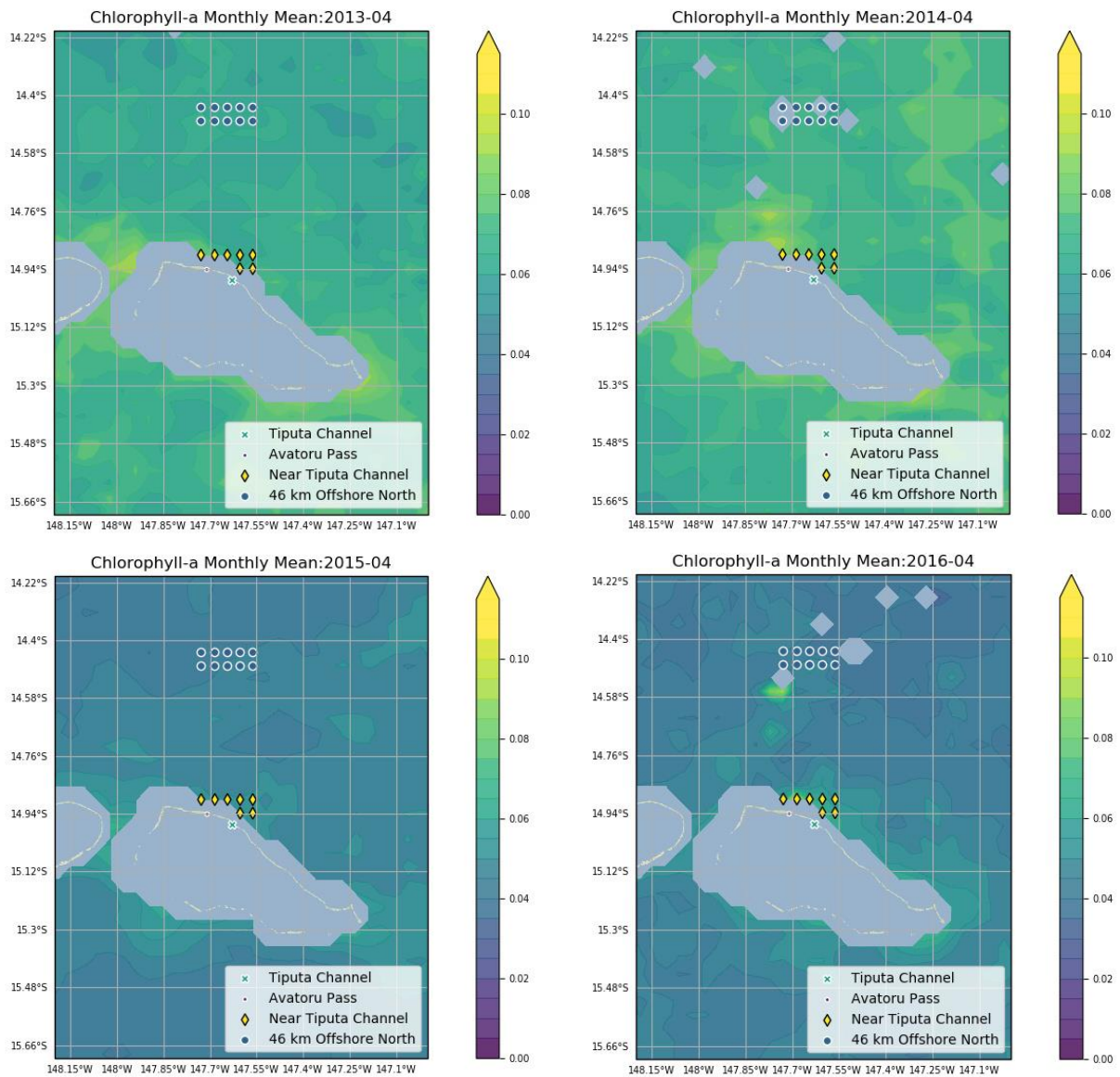


Figure 8: Monthly binned chlorophyll-a was projected onto a terrain map and plotted using filled contours. Chlorophyll-a concentration contours are drawn in 0.005 increments from 0 to 0.12 mg m^{-3} . Study points are marked along with Tiputa Channel and Avatoru Pass. Pixels with land or within the 30-m isotherm are masked. Selected maps are from April 2013, 2014, 2015, and 2016 to provide a visual reference to interannual differences in chlorophyll-a concentrations as well as clear examples of IME near Tiputa Channel.

3.2. Correlations

Seven variables were examined as predictors of IME at Tiputa Channel: sea surface temperature (SST), photosynthetically available radiation (PAR), wind magnitude, wind direction, wave power, wave direction, and the multivariate ENSO index (MEI). These predictor variables were compared to the 317, 8-day period chlorophyll-a data differences (between near Tiputa Channel and 46 km offshore) as the response variable. Each predictor variable is averaged over the same 8-day period as the chlorophyll-a data with no lag between response and predictor variables. Entries missing a value were removed from the dataset, resulting in 310 sets for analysis.

To find relationships between the response and predictor variables the correlation coefficients (r-values) and their significance (p-values) were calculated using pairwise correlation of columns Pearson method (Abbott 2017). The r-values span from 0 to 1, with larger numbers showing a higher correlation. Positive signs indicate a positive correlation, negative signs indicate a negative correlation. The p-values span from 0 to 1 with results less than 0.05 indicating significance.

The highest correlations for chlorophyll-a difference were found with SST and PAR (Figure 9). Chlorophyll-a difference and SST have a positive correlation coefficient (r-value) of 0.15. When temperatures increase the difference between chlorophyll-a near Tiputa Channel and 46 km offshore increases (p-value < 0.05).

The difference between chlorophyll-a (near Tiputa Channel and 46 km offshore) and PAR has a negative correlation coefficient (r-value) of -0.14. When PAR increases the difference between chlorophyll-a near Tiputa Channel and 46 km offshore decreases (p-value < 0.05).

Relationships also exist between the predictor variables. The seasonal pattern of austral summer and winter influence SST, PAR, wind magnitude, wind direction, wave power, and wave direction. Mean SST has a positive correlation with mean PAR (more solar energy, warmer sea surface), wind direction (wind direction is seasonal, from the south in austral winter and more southwesterly the remainder of the year), wave direction (follows the same pattern as wind direction), and MEI (positive MEI during El Niño warming, negative MEI during La Niña

cooling) and a negative correlation with wind magnitude and wave power due to stronger wind and waves in the austral winter when mean SST is lower (r-values Figure 9). The positive relationship between PAR and SST is stronger when SST is lagged behind PAR because it takes time for water to warm up. MEI does not follow the seasonal pattern and has no significant relationships with the mean PAR or wind direction.

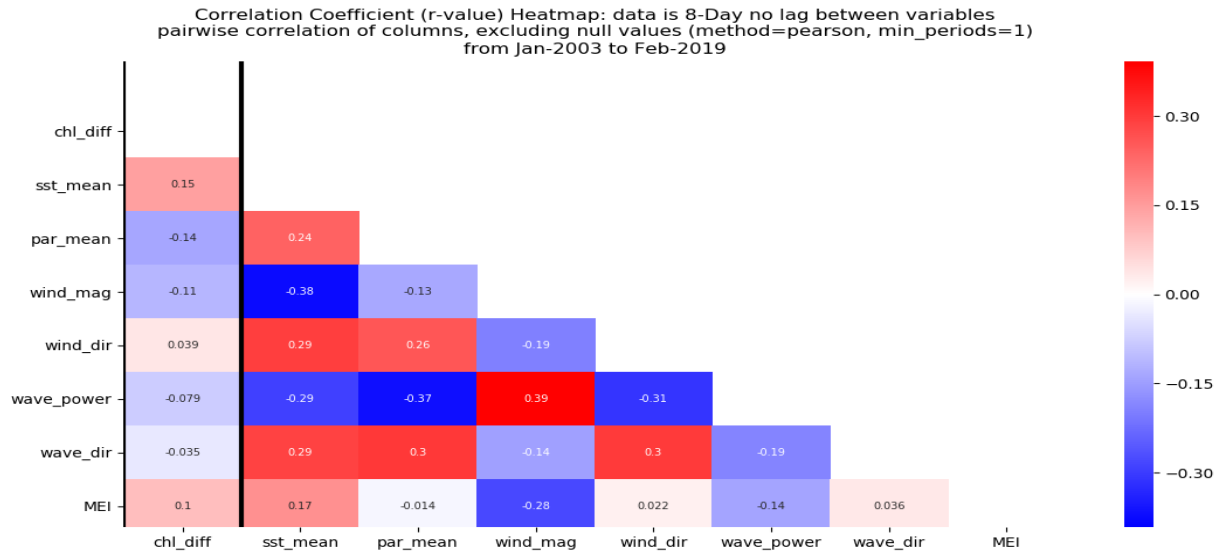


Figure 9. Correlation Coefficient (r-value) heatmap from data between January 2003 to February 2019. The response variable (chl_diff) is the chlorophyll-a data differences between near Tiputa Channel and 46 km offshore. Data are 8-day averages with no lag between variables. The predictor variables are: sea surface temperature (SST) (sst_mean), photosynthetically available radiation (PAR) (par_mean), wind magnitude (wind_mag), wind direction (wind_dir), wave power (wave_power), wave direction (wave_dir), and the multivariate ENSO index (MEI). Colors indicate the correlation coefficient (r-value). Red indicates a positive relationship between variables. Blue indicates a negative relationship between variables. The strength of color indicates the strength of the relationship.

A generalized additive model (GAM1) was developed to examine both the linear and non-linear relationships between chlorophyll-a difference (IME) and its seven predictor variables (SST, PAR, wind magnitude, wind direction, wave power, wave direction, and MEI). The response and predictors are time aligned (no lag) 8-day averages, entries missing a value were removed from the dataset, resulting in 310 sets for analysis.

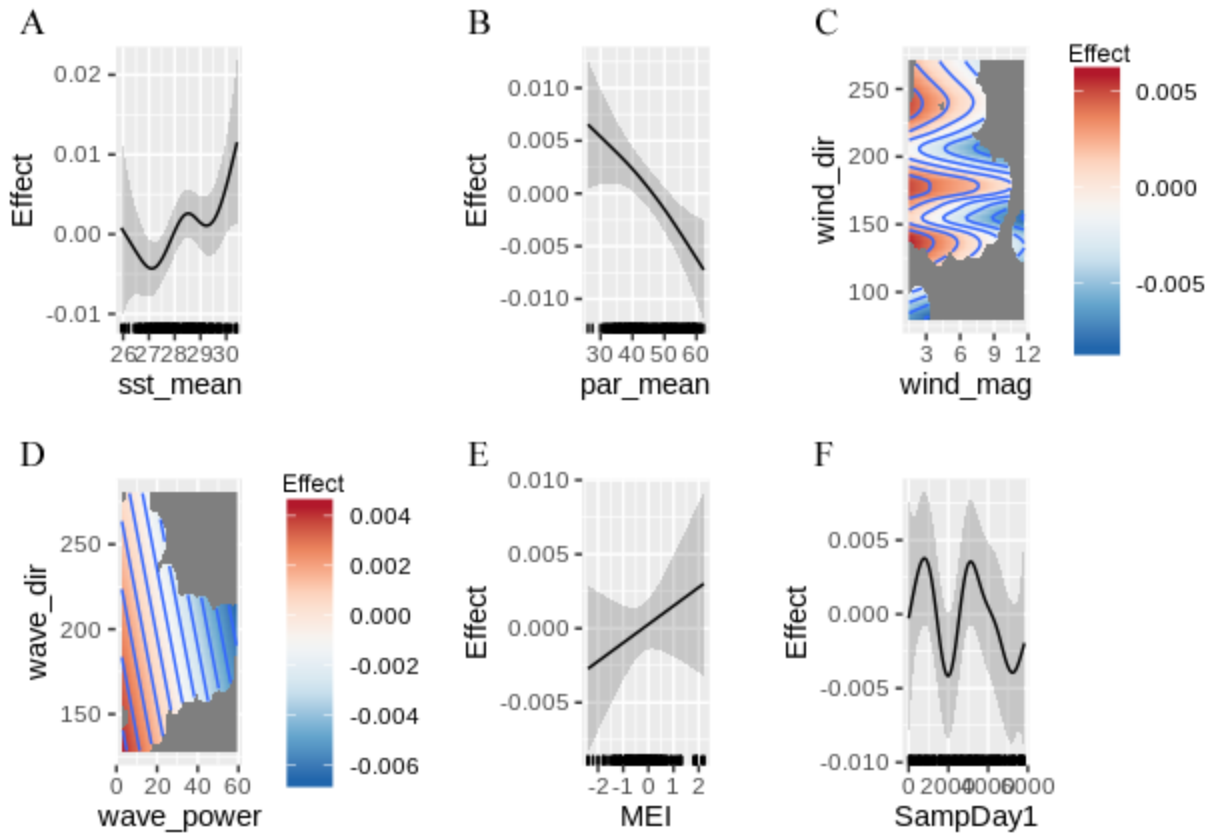


Figure 10. GAM1 results. Data are 8-day averages with no lag between variables excluding null values. Data span from January 2003 to February 2019. The sum of these six panels result in GAM1. 10A. SST (sst_mean) in °C is the x-axis, the y-axis contains the modeled partial response of predictor variable, mean SST, on chlorophyll-a difference between near Tiputa Channel and 46 km offshore. 10B. Same as 10A with predictor variable mean PAR (par_mean) in Einstein m⁻² d⁻¹. 10C. 10E. Same as 10A with predictor variable MEI. 10D. Wind direction (wind_dir) in ° from north is the y-axis, wind magnitude (wind_mag) in m s⁻¹ is the x-axis. The modeled partial effect of these two predictor variables is indicated by the color bar, red indicating positive chlorophyll difference and blue negative. 10E. Wave direction (wave_dir) in ° from north is the y-axis, wave power (wave_power) in kW m⁻¹ is the x-axis. The modeled partial effect of these two predictor variables is indicated by the color bar, red indicating IME. 10F. Same as 10A with predictor variable days since first sample (SampDay1).

GAM1 (Figure 10) explains 19.4% deviance, r-squared of 0.128, and smoothed SST and PAR were both significant (p-value < 0.05). The relationship between IME and SST is non-linear, there is less confidence at both low (< 27 °C) and high (> 29 °C) SST. In the realm of higher confidence, IME and SST have a positive relationship between 27 and 28.5 °C (increasing SST increasing IME) and negative relationship between 28.5 and 29 °C. The relationship between IME and PAR is a negative near-linear relationship (decreasing PAR increasing IME), there is less confidence below 30 Einstein m⁻² d⁻¹. The modeled partial response of chlorophyll-a difference (between near Tiputa Channel and 46 km offshore) to mean SST and mean PAR is shown in Figure 10.

Selecting the best fit model (GAM2) (Figure 11) dropped the variables MEI, wave direction, and wave power. GAM2 explains slightly less deviance at 18.4%, r-squared is 0.126, and smoothed SST and PAR are both significant (p -value < 0.05).

While wind is not significant in either model, the results indicate that higher IME occurs with low magnitude wind at approximately 190° from the north (near the mean conditions). The variable SampDay1, also insignificant, is a variable to avoid temporal auto-correlation.

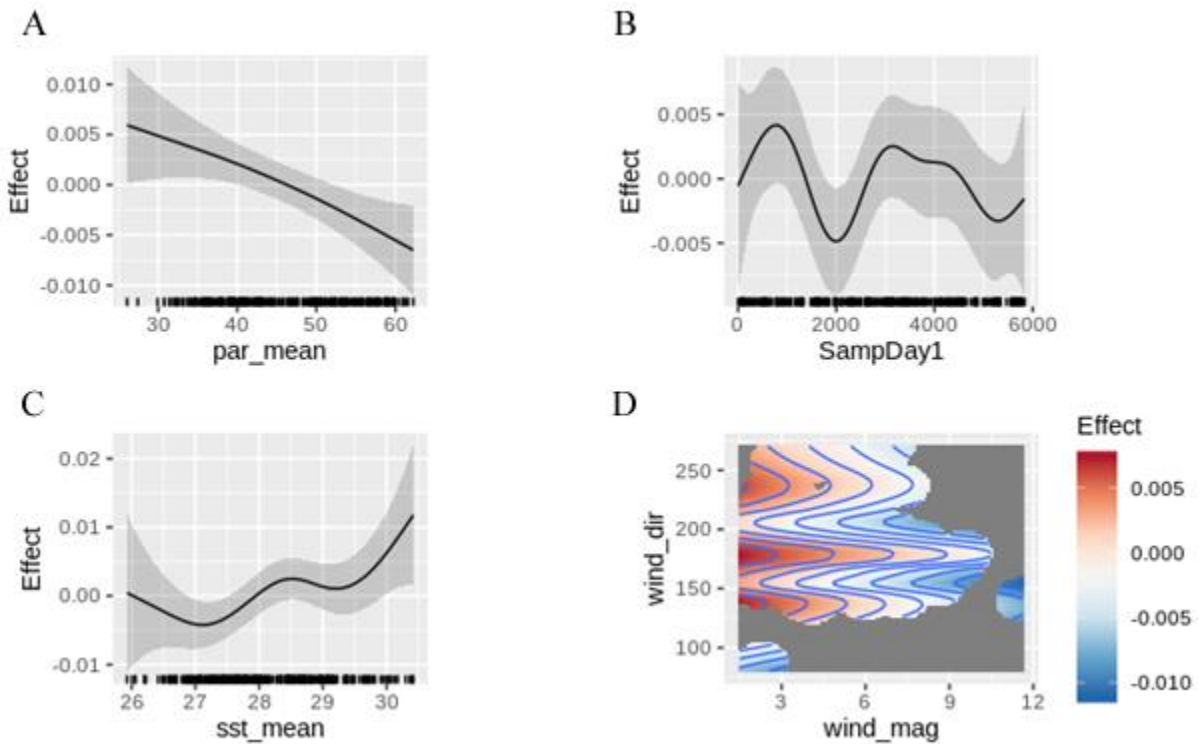


Figure 11. GAM2 results. Data are 8-day averages with no lag between variables excluding null values. Data span from January 2003 to February 2019. 11A. The x-axis contains the predictor variable PAR (par_mean) in $\text{Einstein m}^{-2} \text{d}^{-1}$ the y-axis contains the modeled partial effect of predictor variable, mean PAR, on chlorophyll-a differences between near Tiputa Channel and 46 km offshore. 11B: Same as 11A with predictor variable Sample Day (SampDay1). 11C. Same as 11A with predictor variable SST (sst_mean) in $^\circ \text{C}$. 11D. Wind direction (wind_dir) in $^\circ$ from north is the y-axis, wind magnitude (wind_mag) in m s^{-1} is the x-axis. The modeled partial effect of these two predictor variables on chlorophyll difference is indicated by the color bar, red indicating positive chlorophyll difference and blue negative

3.3. Seasonal Patterns

Sixteen years (January 2003 to February 2019) of 8-day mean data response variables (chlorophyll-a difference (IME)) and predictor variables (sea surface temperature (SST), photosynthetically available radiation (PAR), wind magnitude, wind direction, wave power, wave direction, and the multivariate ENSO index (MEI)) were plotted on the same 8-day increments across a years time to investigate seasonality (Figures 12A-G).

Over this 16 year period, SST ranges from 25.93 to 30.87 °C with a mean temperature of 28.17 °C (Figure 12A). Clear seasonality can be seen in SST following the austral summer and winter pattern. The SST annually dips with the coldest months being July, August, September, and October. The coldest year was 2011 with an annual mean SST of 27.10 °C. The warmest year was 2016 with an annual mean SST of 28.70 °C.

Seasonality can also be seen in PAR with the austral winter constantly having lower levels of PAR from May through August (Figure 12B). PAR levels range from mean 21.37 to 62.37 with a mean value of 45.85 Einstein m⁻²d⁻¹. PAR levels show the most fluctuation during the rainy summer season November, December, January, and February. Lag between PAR and SST can be seen in Figures 12A and 12B, this is because it takes time for water to warm up.

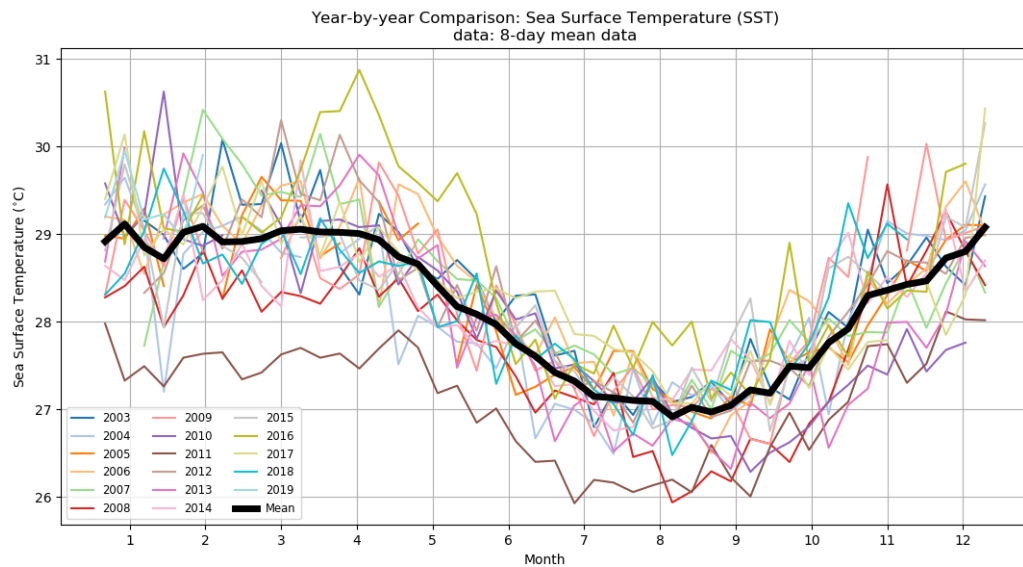
Wind magnitude ranges from 0.99 to 11.63 m s⁻¹ with a mean wind magnitude of 5.76 m s⁻¹ (Figure 12C). The average wind magnitude reached its highest values in July, August and September. Wind direction ranged from 80.15° to 326.40°, with a mean wind direction of 183.97° (Figure 12D). Wind direction gradually shifts through the year from a monthly mean of 168.56° in July to a monthly mean of 204.56° in January.

Wave power ranges from 2.68 to 82.25 kW m⁻¹ with a mean value of 18.47 kW m⁻¹ (Figure 12E). Waves are most powerful in the months surrounding austral winter (May through September), peaking in July with a secondary peak in September of most years. During the austral summer months, waves are less powerful and there is less variability in the wave power over most years. Wave direction ranged from 127.59° to 297.32°, with a mean wave direction of 199.92° (Figure 12F). Wave direction gradually shifts through the year from a monthly mean of 184.01° in

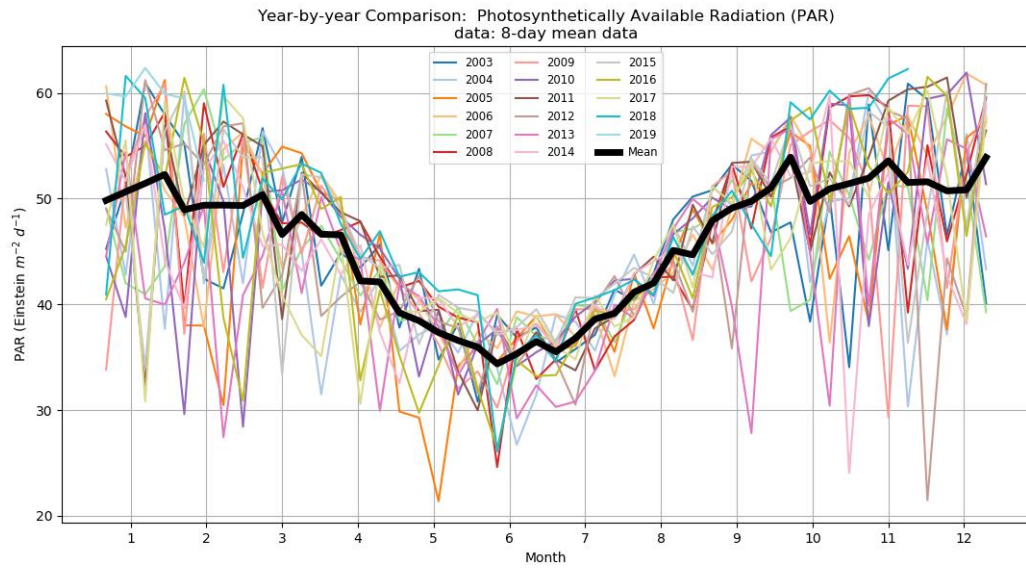
August to a monthly mean of 222.64° in January. Wave climate at Rangiroa is dominated by the austral winter with swells from the south (Figure 12F).

The difference in chlorophyll-a concentration between near Tiputa Channel and 46 km offshore to the north was also investigated between 2003 and 2019, comparing years (Figure 12G). Seasonality was not evident in the strength of the IME. Great variability can be seen when comparing IME across years. The mean value of IME is 0.008 mg m⁻³ with a large standard deviation of 0.015 mg m⁻³. The highest IME value was 0.091 mg m⁻³ in March 2010, September 2012 was the largest difference, -0.043 mg m⁻³, where 46 km offshore was higher than near Tiputa Channel.

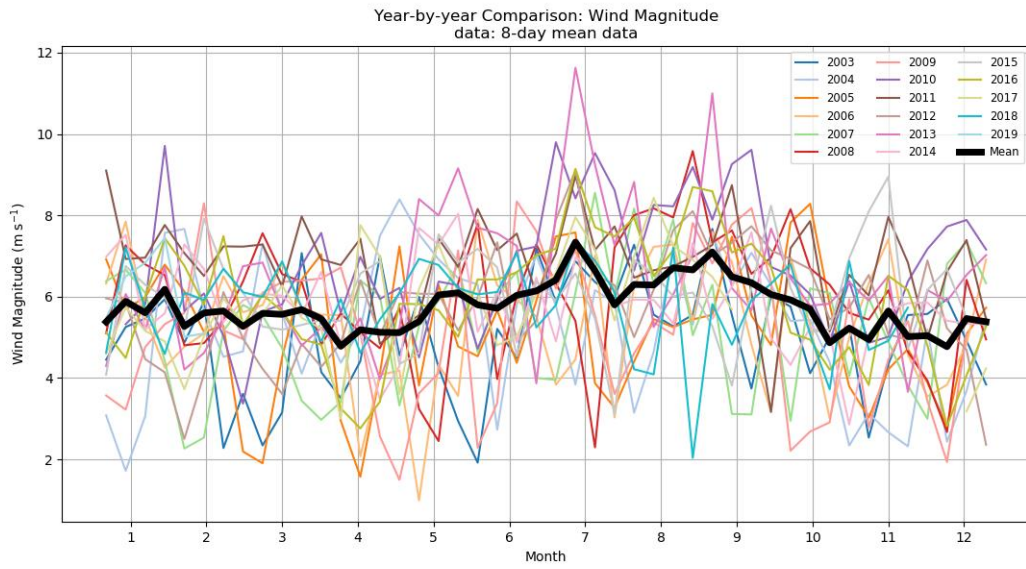
A



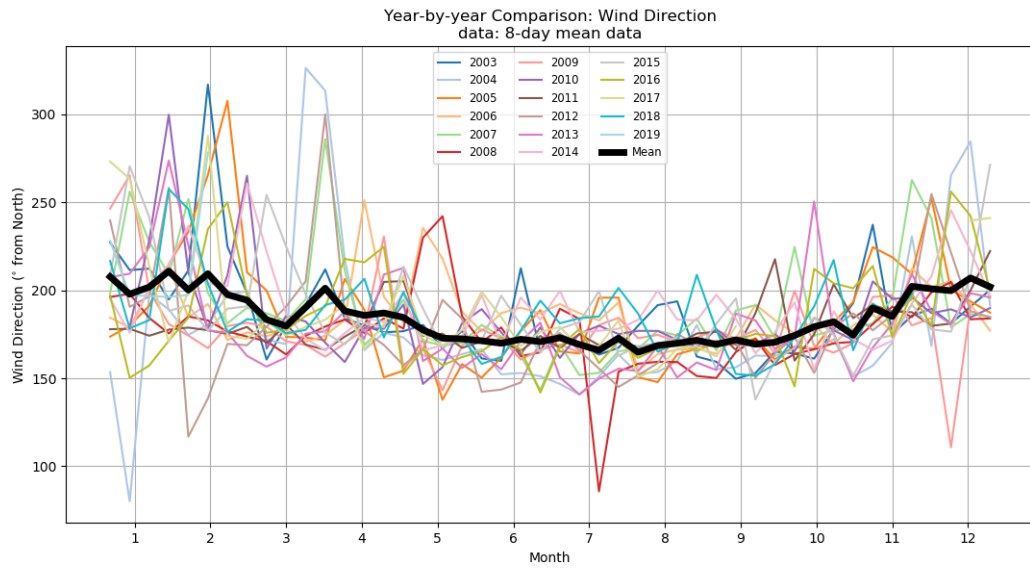
B



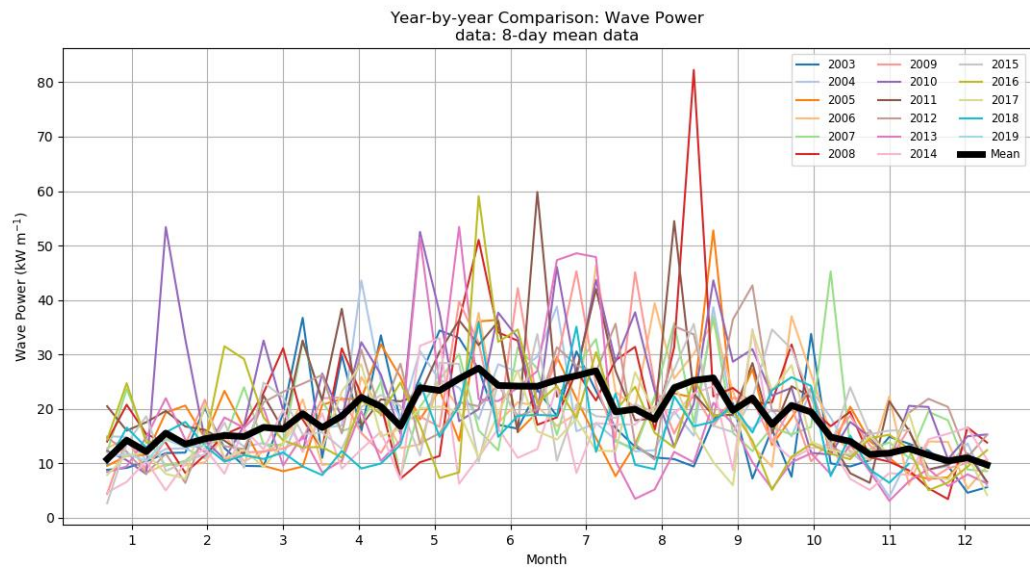
C



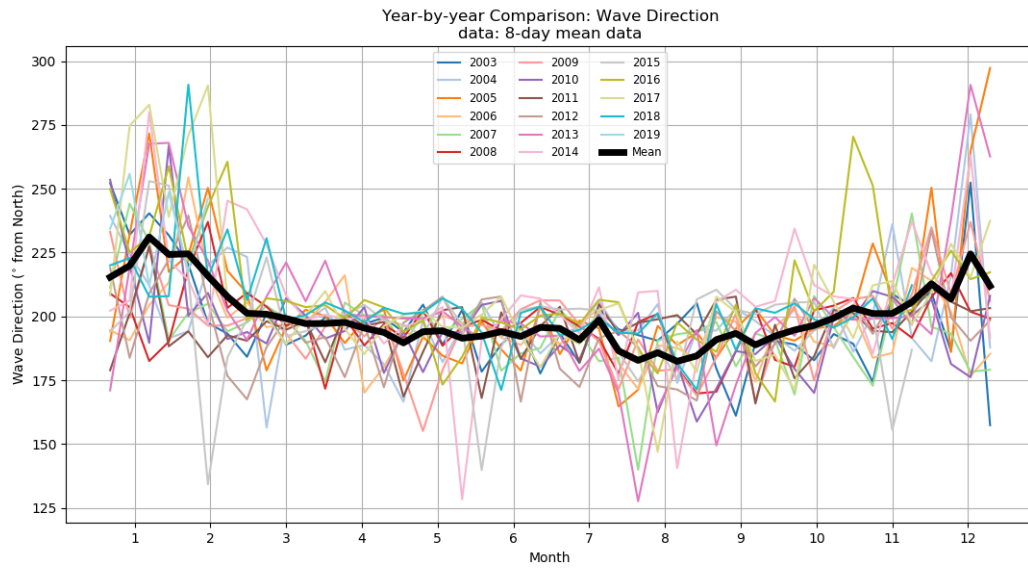
D



E



F



G

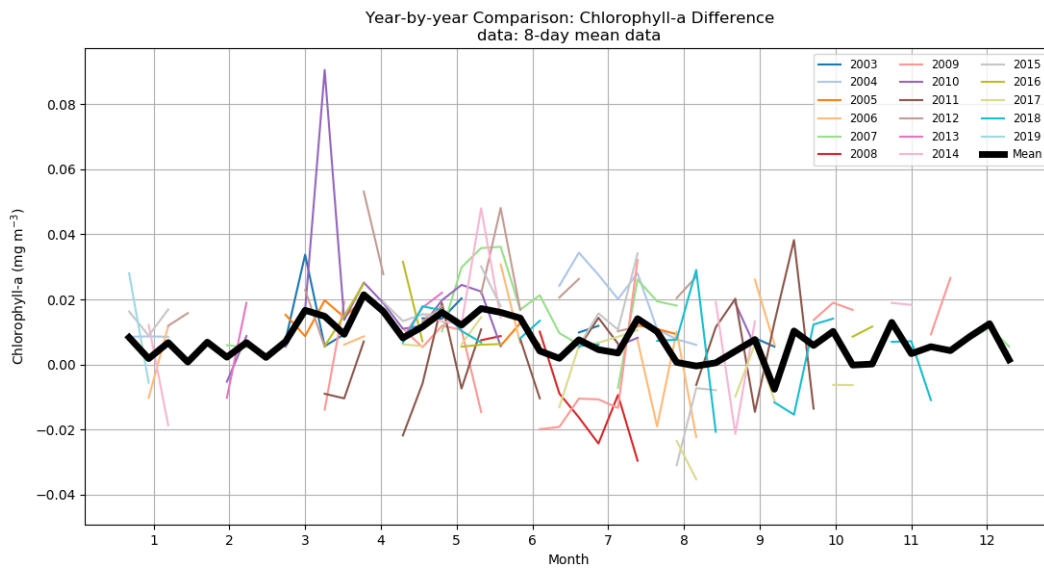


Figure 12. Year by year comparison of 8-day mean values for each predictor variable as well as the response variable (chlorophyll-a difference). Each year has a color coordinated line. The dark black line is the collective mean for all years. Data are 8-day averages. Data span from January 2003 to February 2019. The x-axis is months of the year 1-12. 12A: SST in $^{\circ}\text{C}$ is the y-axis. 12B: PAR in $\text{Einstein m}^{-2}\text{d}^{-1}$ is the y-axis. 12C: Wind magnitude in m s^{-1} is the y-axis. 12D: Wind direction in $^{\circ}$ from north is the y-axis. 12E: Wave power kW m^{-1} is the y-axis. 12F: Wave direction in $^{\circ}$ from north is the y-axis. 12G: Chlorophyll-a difference in mg m^{-3} is the y-axis.

3.4. *In Situ* Observations in Tiputa Channel

PAR, pressure (i.e., water depth), light transmittance, temperature, conductivity (i.e., salinity), and current velocity were measured in Tiputa Channel from April 18 through 22, 2014, at a sampling frequency of 2 minutes.

The effect of tidal forcing in Tiputa Channel was evident during this time. The water level fluctuated with the tides, up to 60 cm. Solar insolation increased shortly after sunrise on each day, and decreased shortly before sunset (Figure 13). The highest level of relative PAR was 0.0026 voltage recorded during the day of April 21 (Figure 13).

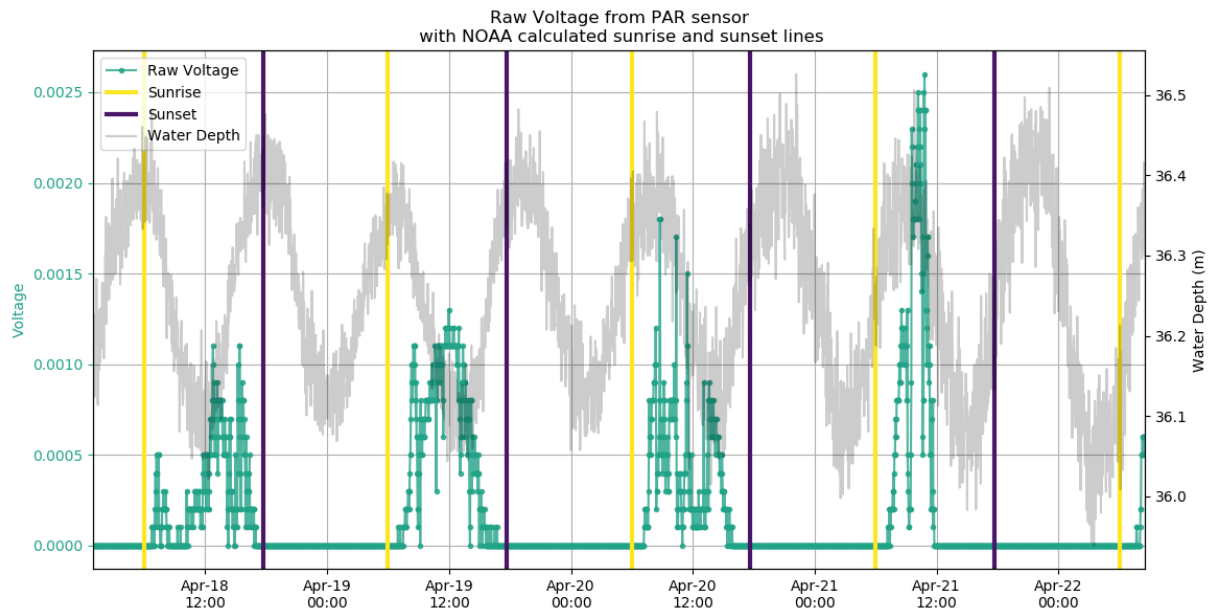


Figure 13. Raw Voltage from BioSpherical Instruments QSP-2200PD PAR sensor. Voltage indicated by aqua line (y-axis left). Yellow lines indicate sunrise. Dark blue lines indicate sunset. Sunrise and sunset are from the NOAA Solar Calculator (<http://www.esrl.noaa.gov/gmd/grad/solcalc/>). Gray line indicates water depth in meters (y-axis right) derived from Sea-Bird Electronics 19plus CTD. Data from mooring C at depth 37 m from 00:00 April 18, 2014 through 12:00 April 22, 2014.

Throughout the deployment, light transmission through the water ranged from 95.28% (lower transmittance) to 99.87% (highest transmittance) with a mean of 97.90% transmittance (Figure 14). Water leaving the atoll on the outgoing ebb tide is less transparent indicating a higher concentration of particulate matter. Ocean water flooding into the atoll approaching high tide allows more light transmittance despite the increased depth, indicating a lower concentration of particulate matter in the water column.

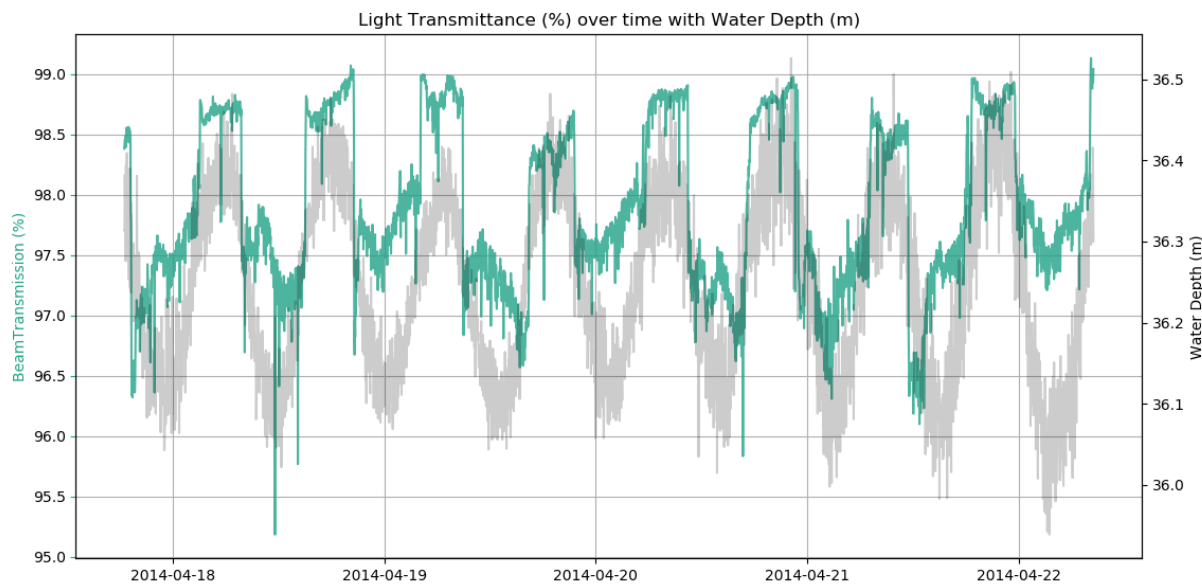
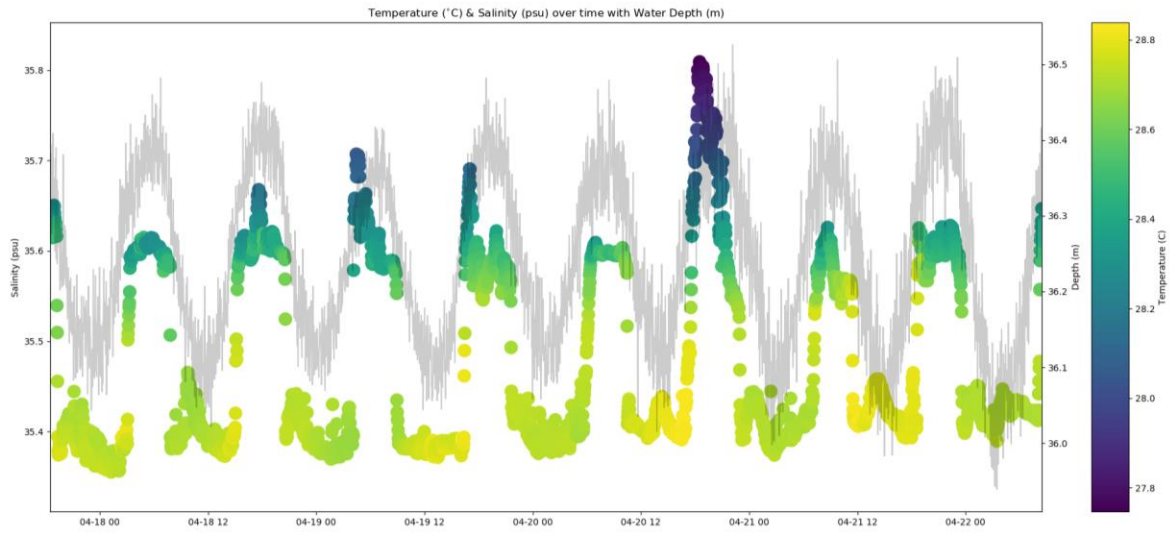


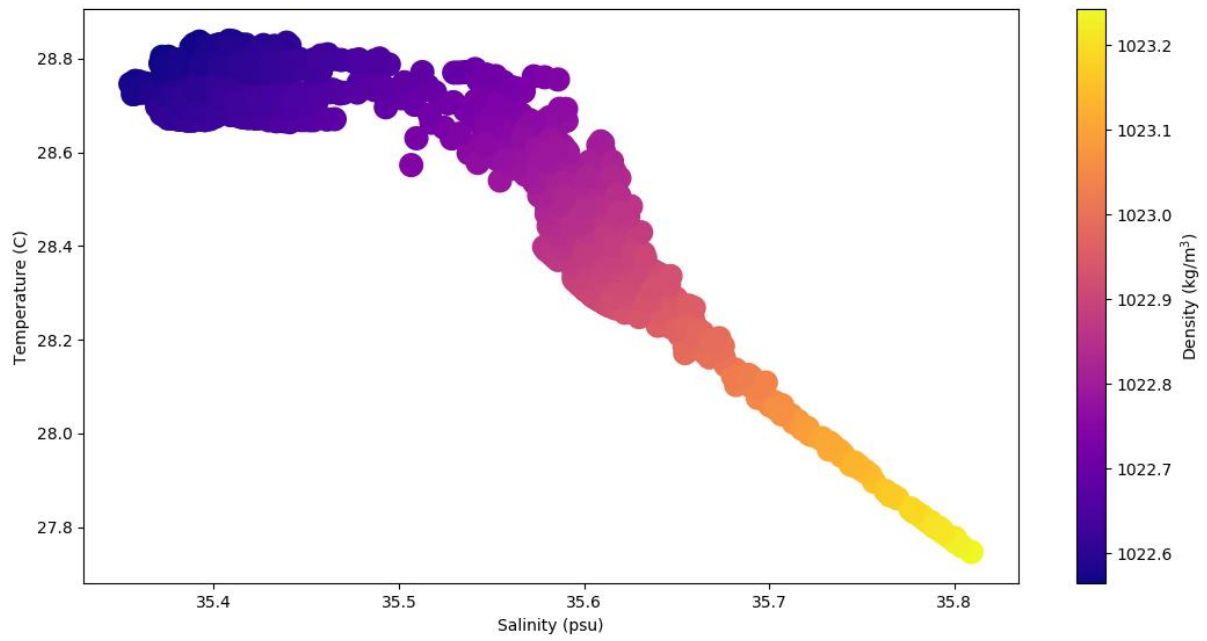
Figure 14. Light transmittance (%) over time with water depth in Tiputa Channel at mooring C. Light transmittance data from Wet Labs C-Star transmissometer. Transmittance (aqua) values (y-axis left). Gray line indicates water depth in meters derived from Sea-Bird Electronics 19plus CTD (y-axis right). Data from mooring C at depth 37 m from April 18, 2014 through April 22, 2014.

Salinity levels at mooring C ranged from 35.36 to 35.81 psu with a mean of 35.48 psu. The temperature ranged from 27.75 to 28.84 °C with a mean of 28.62 °C. The colder, saltier water is more dense than the warmer, less salty water. Density ranges from 1022.56 to 1023.24 kg m⁻³ with a mean density of 1022.71 kg m⁻³. Water flowing into the atoll on the flood tide is colder, saltier, and more dense than water flowing out of the atoll with the low tide (Figure 15A). Over the 5 day span, April 18-22, 2014, 48 mm of precipitation fell on the far west of the lagoon. Lower rainfall amounts were recorded over the remainder of the atoll ranging from 12 mm in the far east upward to 48 mm in the far west (Figure 15C). This precipitation did not have a notable effect on the measured salinity values in Tiputa Channel.

A



B



C

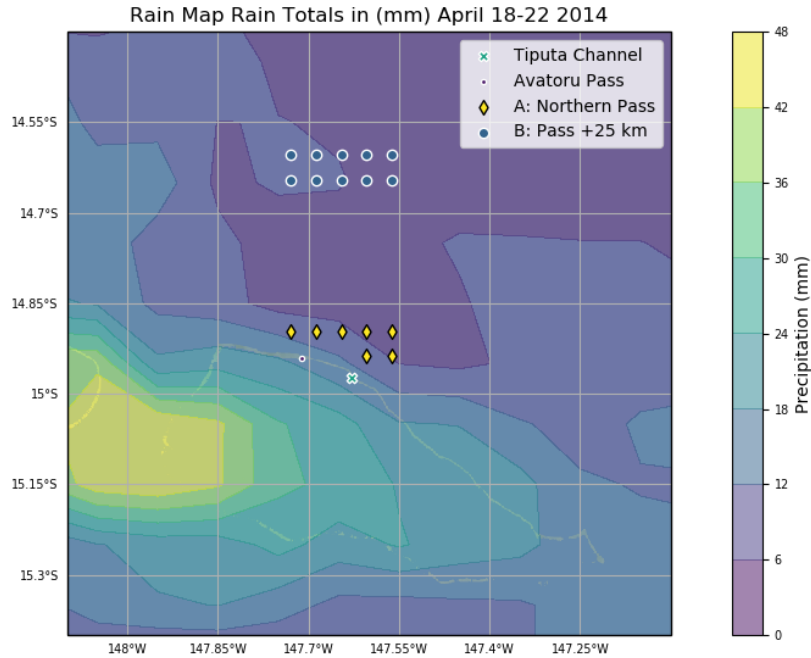


Figure 15A. Temperature and salinity plotted with water depth over time from mooring C from April 18 to 22, 2014. Color indicates temperature in °C with yellow being warmer and blue colder. Salinity in psu (y-axis left). Water depth in m indicated by gray line (y-axis right). Time along x-axis. Temperature, salinity, and pressure data from Sea-Bird Electronics 19plus CTD. 15B: Temperature, salinity, and density. Same data set as 15A. Temperature in °C values on y-axis left. Salinity in psu values on x-axis. Colors indicate density in kg m^{-3} with yellow being more dense and blue less dense. 15C: Total cumulative rain in mm during the study period April 18 to 22, 2014 projected onto a terrain map and plotted using filled contours. Yellow indicates high rain, dark blue indicates low or no rain. Rain data from Global Precipitation Measurement (GPM) mission, version 5.

Horizontal currents at moorings A, B, and C flowed in the along channel direction, oriented at 32.2° (true) (northeast) outgoing/ebb, and 212.2° (true) (southwest) incoming/flood. Current flow at the three moorings was predictable, primarily following the tide (Figure 16). Currents are outgoing during ebb tide and incoming during flood tide. Outgoing (ebb) current speeds were faster than incoming (flood) given the additional pressure gradient between the lagoon and the ocean (Table 4). During the sensor deployment period, the maximum outgoing current speed was 2.594 m s^{-1} recorded at mooring B; the maximum incoming current speed was 1.813 m s^{-1} recorded at mooring A.

Vertical currents in Tiputa Channel are weaker than the horizontal currents (Figure 17). The maximum recorded upward flow was 0.292 m s^{-1} at mooring A and maximum downward flow was 0.298 m s^{-1} at mooring B. Downward flow was relatively weak at mooring A at 0.140 m s^{-1} . At mooring B the water at 16.5 m depth follows the tidal signal, current flows upward with flood

tide and downward with ebb tide. Moving from mooring A to B the channel narrows and the seafloor depth drops from 22.5 m to 25.9 m, continuing to mooring C the channel opens to the ocean and seafloor depth continues to drop to 38.0 m; a drop of 15.5 m between moorings A and C spaced 0.4208 km apart.

Table 4. Measurement of current velocity at moorings A, B and C. Current speeds in m s^{-1} .

	Mooring A	Mooring B	Mooring C
max out	2.594	2.636	2.556
max in	-1.813	-1.444	-1.215
max up	0.292	0.267	0.238
max down	-0.140	-0.298	-0.211
mean out	1.467	1.393	1.323
mean in	-0.931	-0.675	-0.582
mean up	0.028	0.053	0.038
mean down	-0.016	-0.084	-0.033

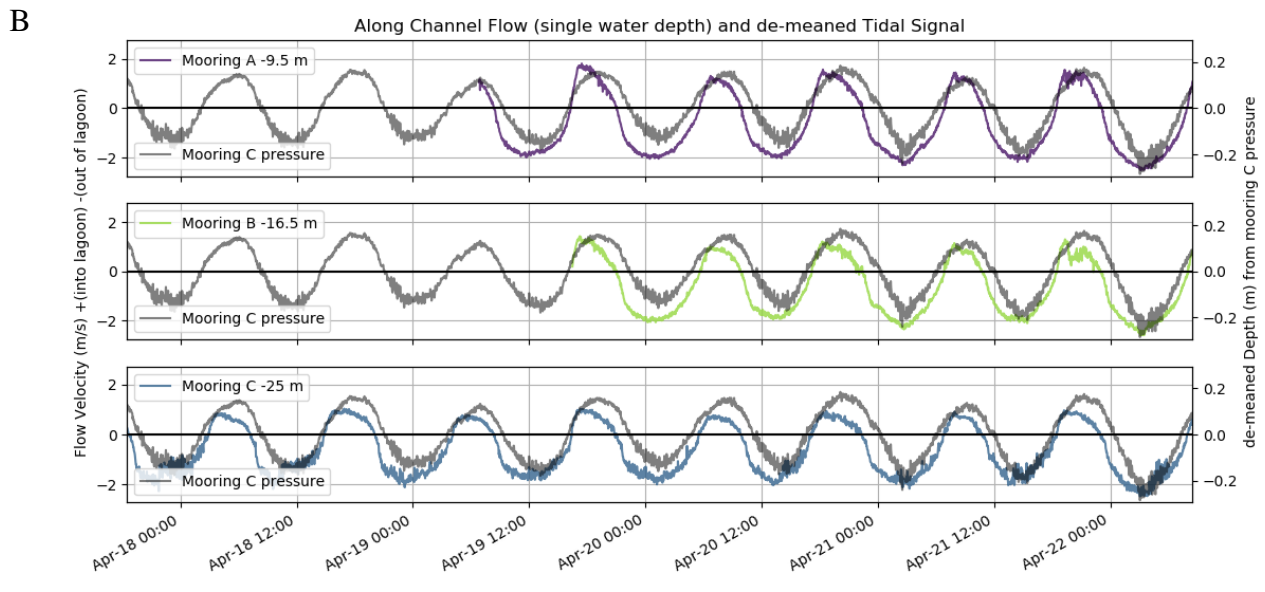
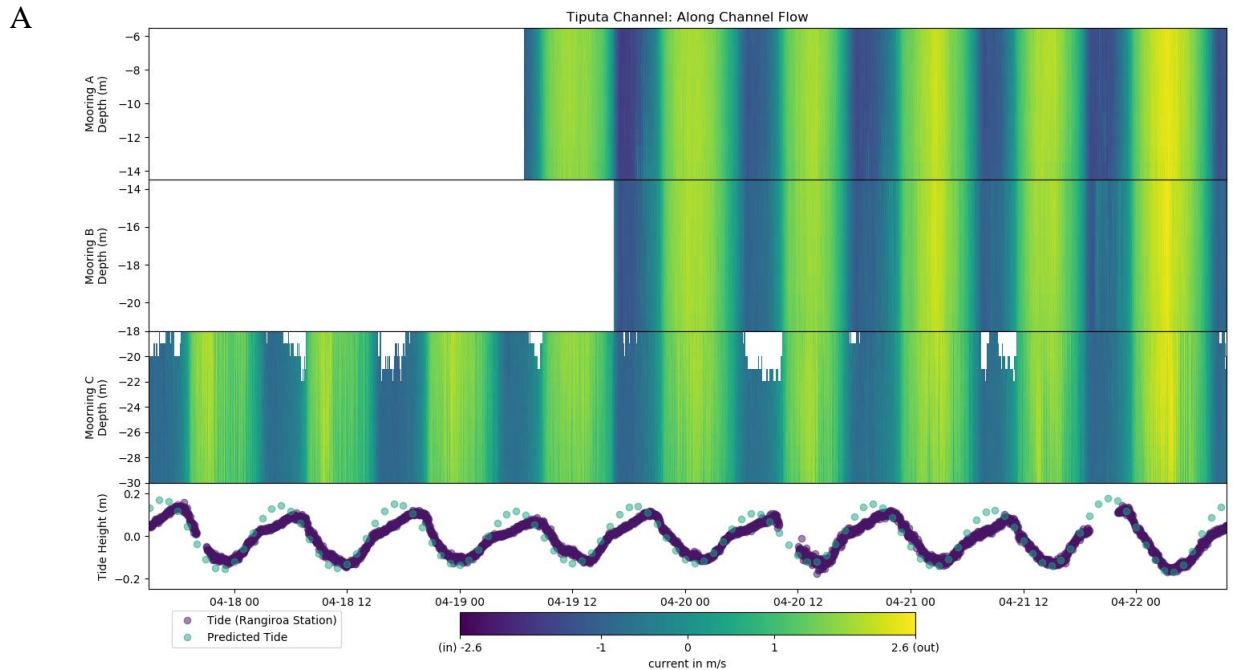


Figure 16A. Horizontal channel flow in Tiputa Channel and sea level during study period 18-22 April 2014. Top three panels show the horizontal current flow at moorings A, B, and C. Yellow indicates water moving out of the atoll lagoon and dark blue indicates water moving into the atoll lagoon. Mooring specifications Table 2, locations Figure 2. Fourth panel shows predicted tide from Oregon State University TPXO <http://wolkov.oce.oorst.edu/tides/global.html> (light blue dots) and recorded sea level measured by the Intergovernmental Oceanographic Commission sea level gauge (dark blue) location Figure 1B. 16B: Horizontal channel flow at single water depth plotted with a demeaned tide taken from pressure at mooring C (gray line in each panel). Top panel is mooring A, flow is at 9.5 m depth (purple). Middle panel is mooring B, flow is at 16.5 m depth (green). Bottom panel is mooring C, flow is at 25 m depth (blue). Time is along x-axis. Flow velocity in m s^{-1} is along left y-axis, positive is upward flow and negative is downward flow. Relative water depth m (y-axis right).

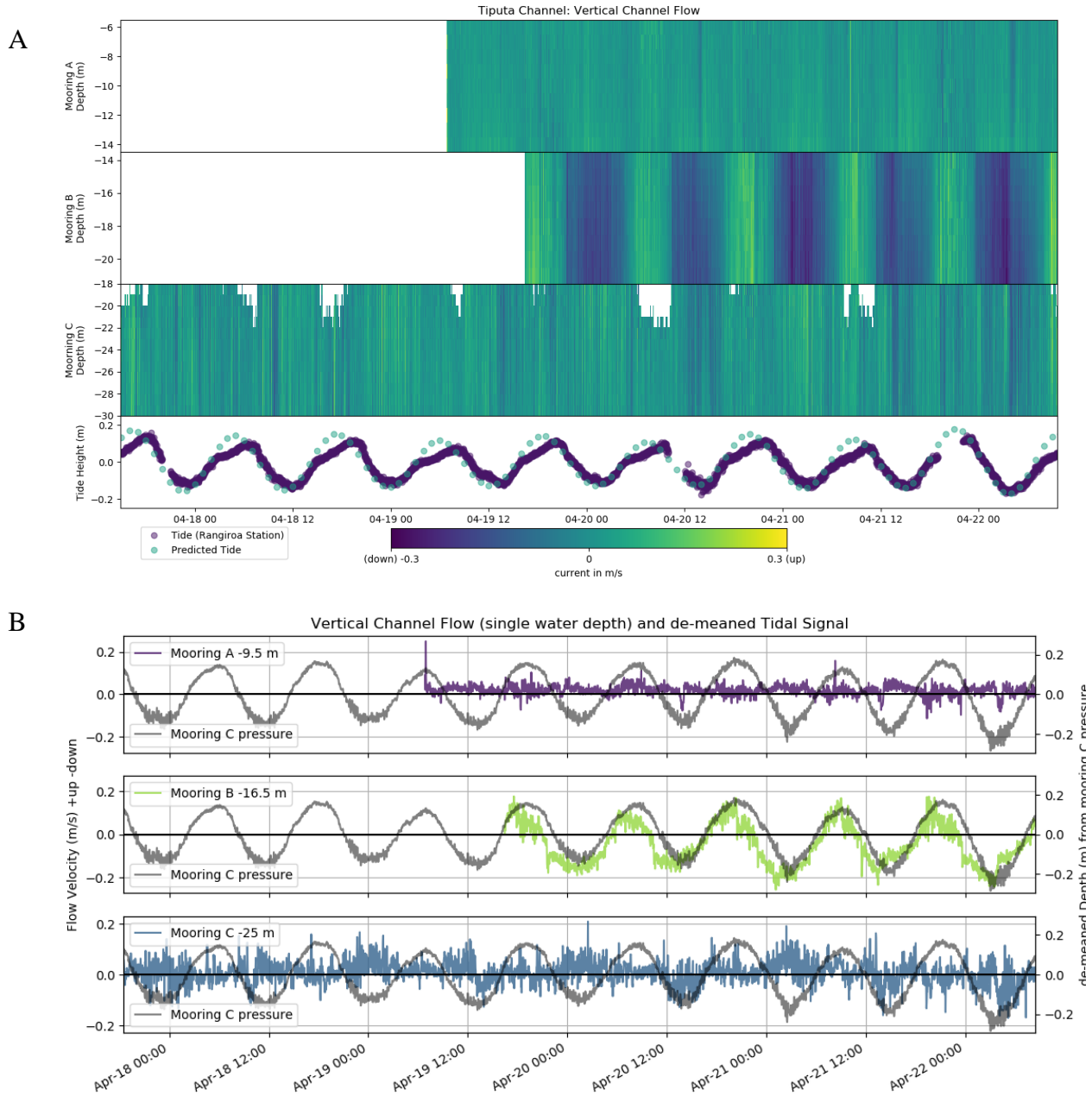


Figure 17A. Vertical channel flow in Tiputa Channel and sea level during study period 18-22 April 2014. Top three panels show the vertical current flow at moorings A, B, and C. Yellow indicates water moving upward and dark blue indicates water moving downward. Mooring specifications Table 2, locations Figure 2. Fourth panel shows predicted tide from Oregon State University TPXO <http://wolkov.oce.orst.edu/tides/global.html> (light blue dots) and recorded sea level measured by the Intergovernmental Oceanographic Commission sea level gauge (dark blue) location Figure 1B. 17B Vertical channel flow at single water depth plotted with a de-meanned tide taken from pressure at mooring C (gray line in each panel). Top panel is mooring A, flow is at 9.5 m depth (purple). Middle panel is mooring B, flow is at 16.5 m depth (green). Bottom panel is mooring C, flow is at 25 m depth (blue). Time is along x-axis. Flow velocity in m s^{-1} is along left y-axis, positive is upward flow and negative is downward flow. Relative water depth in m (y-axis right).

Net water exchange through Tiputa Channel was calculated over a 24-hour period using the along channel flow recorded at mooring B after Moehlenkamp et al. (2019). Mooring B was chosen for its central location in the channel and its constant cross-channel depth. Using the bathymetry data, points on either side of the channel were selected where the depth exceeded 25m. The channel at mooring B is approximately 29.5 m deep by 175 m across. The rate of flow for each time point was averaged over the recorded water column measurements (23 bins with 1 m vertical spacing, from a depth of 4.5 m to 26.5 were averaged to a single flow rate). This flow rate was then applied to the entire depth of 29.5 m. (Flux = Width \times Depth \times Velocity). Since the depth of the water changes with tidal flow, depth varied each time point. Depth was calculated using the pressure sensor from mooring C because the measurements were taken at the same 120 second time interval and the location is closer than Rangiroa Station, mooring C provides a more accurate tidal change measurement for the channel. Net water exchange between Rangiroa lagoon and the ocean was 1,840,000 m³ for the 24-hour period April 20, 2014 00:00 through 23:59 (static net water exchange: 1,850,000. m³ calculated with constant depth of 29.5 m). Water balance over the 24-hour period had 969,000 m³ entering the atoll and 2,810,000 m³ exiting the atoll. Significantly more (2.9 times) water ebbs (exits) the channel, than floods (enters) the channel with a similar tidal excursion. The additional water exiting the atoll is from wave forcing of water over the fringing reef. During the flood tide, as the water level increases so does the volume flux, until reaching the midpoint or highest water level at which point it decreases. On ebb tide the flow is reverse following the same pattern (Figure 18).

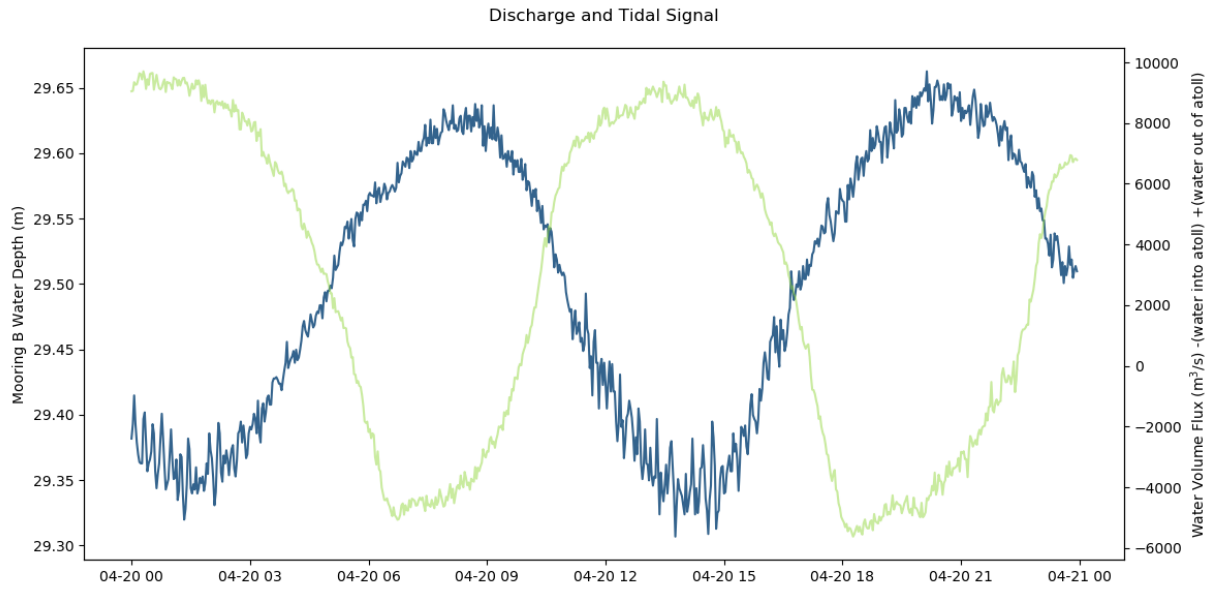


Figure 18. Water level (m, blue, y-axis left) and water flux ($\text{m}^3 \text{s}^{-1}$, green, y-axis right) at mooring B over 24 hour period April 20, 2014. Negative water flux indicates water flowing into the lagoon, positive water flux is flowing out of the lagoon.

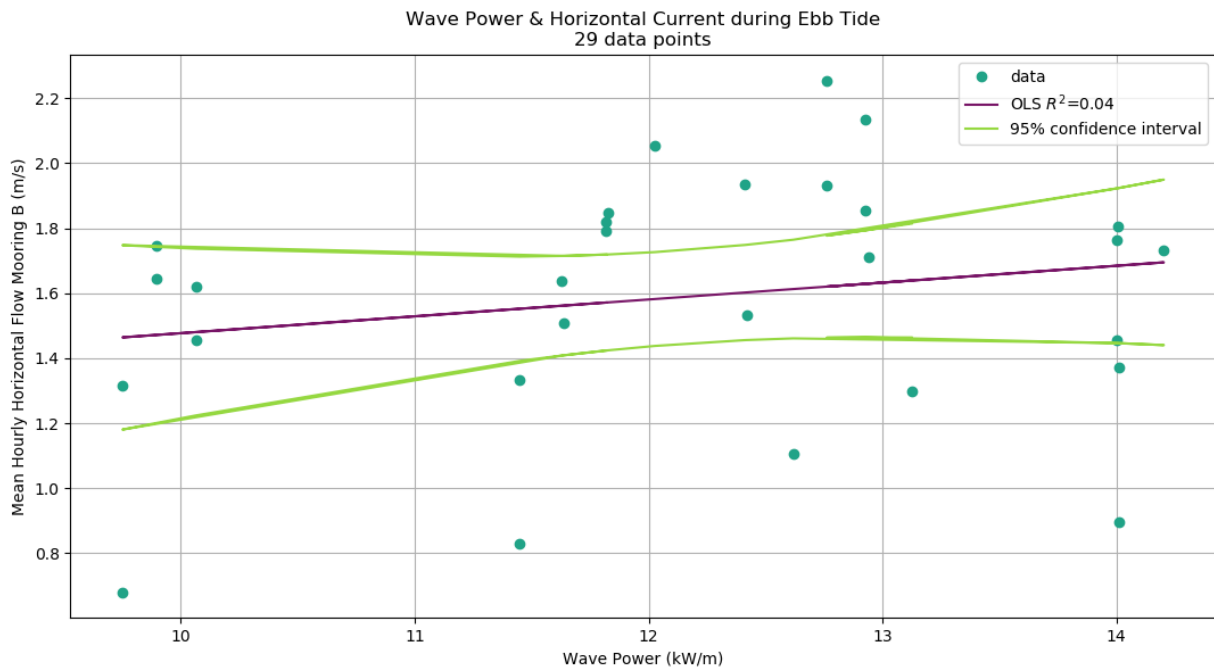


Figure 19. Mean horizontal current and wave power during ebb tide. Hourly averages of current in m s^{-1} from mooring B April 19, 2014 17:00 through April 22, 2014 0800 were plotted against WaveWatch III hourly wave power in kW m^{-1} (blue dots). Ordinary least squares linear regression fit line (purple). 95% confidence intervals (light green).

The hourly mean of the horizontal current at mooring B was compared to hourly wave power during ebb tide (Figure 19). Over the deployment period of mooring B, 29 hourly mean points occur at ebb tide. Faster current flow can be observed with higher wave power. This association is mild (r squared values of 0.04), a longer time period with more variable levels of wave power would likely provide a stronger relationship. Pagès and Andréfouët (2001) also note that the net outflow of Tiputa Channel increases with wave heights above 1.4 m.

From the April 2014 Tiputa Channel data, it is clear that more water exits the atoll through the channel than enters at each tidal cycle. Light transmittance decreases on the outgoing tide. Outgoing water is warmer, less salty, and less dense than incoming ocean water.

3.5. Additional Tests and Data

In addition to the results identified throughout this thesis, there were several tests, as well as additional data that were explored which yielded no significant results (Table 5).

Lagging the predictor variables (SST, PAR, wind magnitude, wind direction, wave power, wave direction, and MEI) one 8-day period behind the response variable (chlorophyll-a difference) was tested. Pearson's pairwise correlation was performed against the response and lagged variables, the positive relationship between chlorophyll-a difference and SST slightly strengthened, there was no other significant change (r-value 0.18 for 8-day lagged SST, compared to r-value 0.15 0-day lag).

In addition to examining chlorophyll-a near Tiputa Channel and 46 km offshore to the north, chlorophyll-a was also investigated at three additional locations: 23 km offshore to the north, near the southern fringing reef, and 23 km to the south of the southern fringing reef. Chlorophyll-a at all five locations followed the same general pattern (as seen with near Tiputa Channel and 46 km offshore north in Figure 6, additional three locations not shown). Using the Mann Whitney U Test sets were compared (1) chlorophyll-a measurements 23 km north, 46 km north, and 23 km to the south of the atoll were found to be statistically of the same set, eliminating the sets 23 km north and south (2) chlorophyll-a measurements near Tiputa Channel and near the southern fringing reef were found to be statistically of the same set, eliminating the set near the southern fringing reef.

Initial chlorophyll-a investigation was performed on daily satellite data over a shorter time span, from January 1, 2012 through December 31, 2017, with four predictor variables: wave power, wave direction, wind magnitude, and wind direction. The three paragraphs below describe the tests performed with this data set.

Chlorophyll-a daily data were used to look for higher resolution relationships with wind and wave parameters. Individual plots were made to visually inspect for patterns. The 20 largest, as well as the 20 smallest chlorophyll-a differences, were identified and plotted with seven days of preceding wind and wave data. This was done to see if the changes in wind or wave forcing

were responsible for high or low chlorophyll-a differences. In addition to the visual inspection of lagged wind and wave data, Pearson's pairwise correlation was also run for wind and wave data lagged behind chlorophyll-a difference between 1 and 20 days with no significant results.

Chlorophyll-a daily data were used to look at chlorophyll-a differences over time. The highest 10 and lowest 10 chlorophyll-a difference values of each year were examined, this was done to look for patterns in the yearly extreme values. No patterns were found, highs and lows of chlorophyll-a difference occurred throughout the year with no strong patterns over the 16 year span.

High power wave events (defined as periods where wave power was greater than the mean plus two standard deviations) were identified. Daily chlorophyll-a differences were identified surrounding high wave power events, however, due to satellite coverage as well as cloud blockage there were no dates with chlorophyll-a data measured the day before, the day of, and the day after the wave events. Further, there was no clear positive or negative trend in chlorophyll-a in the days following high power wave events.

Table 5. Additional tests and data explored with no significant results.

Test or Data Examined	Data Frequency	Results
Pearson's pairwise correlation lag all predictor variables by one 8-day period.	8-day	SST r-value increased from 0.15 to 0.18
Chlorophyll-a at other locations: 23 km north of Tiputa Channel 23 km south of atoll near southern fringing reef	8-day	Other locations found to be statistically similar to study locations
Visual pattern inspection of the highest 20 chlorophyll-a differences plotted with wind and wave parameters.	Daily	No patterns found
Visual pattern inspection of the lowest 20 chlorophyll-a differences plotted with wind and wave parameters.	Daily	No patterns found
Pearson's pairwise correlation with highest 20 chlorophyll-a differences lagged 1-20 days.	Daily	No significant results
Pearson's pairwise correlations with lowest 20 chlorophyll-a differences lagged 1-20 days.	Daily	No significant results
Highest 10 chlorophyll-a differences per year plotted over the 6-year time span sorted by month.	Daily	No significant results
Lowest 10 chlorophyll-a differences per year plotted over the 6-year time span sorted by month.	Daily	No significant results
Inspect chlorophyll-a before and after high power wave events.	Daily	No patterns found

4. DISCUSSION

4.1. The Island Mass Effect

The IME is present in the waters outside Tiputa Channel, Rangiroa Atoll 75.7% of the time over a 16-year period. During this period the chlorophyll-a concentration was 16% higher on average than the surrounding ocean. On average, the IME in the waters outside Tiputa Channel is 0.015 mg m⁻³ higher than 46 km offshore. For the 24.3% of the time when chlorophyll-a concentration 46 km offshore is higher than the waters outside Tiputa Channel the difference is smaller with an average of -0.013 mg m⁻³. The periods of time when chlorophyll-a concentration is higher 46 km offshore may be caused by localized changes in the open ocean that increase chlorophyll-a offshore (i.e., a mesoscale feature resulting in higher chlorophyll-a biomass near the offshore location).

The in-water sensors measured warmer, fresher, less transparent water exiting the atoll at each ebb tide. The monthly satellite data from April of 2014 corresponding to the time frame the *in situ* data were collected reveals that the average chlorophyll-a concentration in the coastal waters just outside Tiputa Channel were higher in chlorophyll-a than in the ocean 46 km to the north. This suggests that Rangiroa lagoon provides a source of nutrients, particulates, and chlorophyll-a into the surrounding oligotrophic ocean. The sources of nutrients, particulates, and chlorophyll-a are likely due to water exchange over the reef, benthic processes increasing available nutrients in the lagoon, as well as a long residence time. When warmer, less saline, lower density water from the atoll containing higher nutrients and particulates are advected into the coastal ocean the combination of stratification and fuel for phytoplankton likely produces the increased chlorophyll-a evident in the satellite data (Kirk 2011).

In a ten year study of IME across the tropical Pacific, Gove et al. (2016) found an increase of phytoplankton biomass in 91% of the 32 islands and atolls surveyed. Examining the islands and atolls exhibiting IME, Gove et al. (2016) found that the intensity of chlorophyll-a enhancement above oceanic levels varied greatly (from 0.2 to 85.6%). Increased magnitude of IME in the Gove et al. (2016) study was found to be linearly related to the geomorphic type (stronger IME at atolls compared to islands), bathymetric slope (stronger IME with a gentle slope than a steep

slope), reef area (stronger IME with more reef area), and population status (stronger IME at populated locations). To determine the total chlorophyll-a throughout the water column, Gove et al. (2016) multiplied the mean satellite-derived chlorophyll-a by the depth of light penetration for each satellite pixel. To ensure that the surface chlorophyll-a was reflective of increases throughout the water column, Gove et al. (2016) used ship-based *in situ* measurements for verification at 29 of the survey locations. While I found an average of 16% increase in chlorophyll-a near Tiputa Channel, it is important to remember this was for satellite detected surface chlorophyll-a in a limited area outside Tiputa Channel and that the increase could be higher if subsurface waters were also considered.

Satellite and *in situ* data suggest that IME occurs at Rangiroa near Tiputa Channel, however the uncertainty of error inherent in satellite chlorophyll-a data must also be addressed. Moore et al. (2009) investigated the standard NASA MODIS chlorophyll-a error of 35% by separating the global oceans into optical types and then defining uncertainty for each water type. Moore et al. (2009) found average relative error to be 16% for clear blue ocean gyre water, but all other water had a higher than 35% relative error. In a 2016 study by Brewin et al. MODIS chlorophyll-a data were compared to *in situ* measurements taken while underway traveling through the center of the Atlantic, in this way they were able to compare a larger geographical average to the corresponding satellite pixel. Using this method Brewin et al. (2016) found the root mean square error of about 0.16. MODIS Chlorophyll uncertainty is lowest in clear oligotrophic ocean and highest near coasts. To reduced satellite chlorophyll-a error associated with coastal measurements, pixels within 3.27 km of the 30-m isobath were excluded in this study of Rangiroa following Gove et al. (2016). Exact uncertainty levels for the satellite chlorophyll-a pixels near Tiputa Channel and 46 km offshore could be estimated with *in situ* sampling of chlorophyll-a in the regions. If we assume the error is 35%, in the 310 sets of chlorophyll-a difference available for analysis, only one set had a chlorophyll difference that was greater than the calculated error. It therefore cannot be said with certainty that IME occurs at Rangiroa near Tiputa Channel. However, there is clearly a pattern of enhanced chlorophyll-a over the 16-year period and *in situ* data supports an export of a water mass capable of increasing phytoplankton outside Tiputa Channel.

Sources of Nutrients in Rangiroa Atoll

Rangiroa Atoll is situated in the oligotrophic ocean. Increased nutrients are required to support the enhanced chlorophyll-a biomass. These nutrients may be supplied to Rangiroa Lagoon from a variety of sources: the benthic fauna in the lagoon, the atoll land, or deep nutrient-rich ocean water. While there has been no direct study of the lagoon nutrients in Rangiroa, studies of other atolls and islands are relevant in explaining increased nutrients.

Several studies have examined the sources and abundance of nitrogen, an important nutrient in primary production, in neighboring Tikehau Atoll Lagoon (Charpy et al. 2012, Charpy-Roubaud et al. 1996, Charpy-Roubaud et al. 2001). Tikehau Atoll Lagoon was estimated to have up to 6.8% of lagoon primary production nitrogen requirements made available from the nitrogen flux at the water-sediment interface (Charpy-Roubaud et al. 1996). An additional source of organic nitrogen in Tikehau Lagoon was benthic nitrogen fixation, accounting for 24.4% of benthic primary production requirements (Charpy-Roubaud et al. 2001). The remainder of Tikehau Lagoon's organic nitrogen requirement was attributed to planktonic nitrogen fixation and external sources (Charpy-Roubaud et al. 2001).

It is likely that there is a limited influx of terrigenous input to the Rangiroa lagoon given the flat terrain and lack of rivers. Charpy-Roubaud et al. (1990) state that there is no terrestrial nutrient input into the lagoon from flat atoll surfaces.

Physical processes have been shown to advect deep, nutrient-rich ocean water to the surface. For example, divergence of flow around steep island/atoll systems may cause upwelling of deeper nutrient-rich water near coasts (Caldeira et al. 2002; Spall and Pedlosky 2013). In addition, internal wave breaking due to abrupt changes in topography may cause pulses of nutrient-rich deep water to be advected up coastal slopes (Leichter et al. 2012).

4.2. Effects of Physical Forces on IME

Two statistical methods, Pearson's pairwise correlation and a general additive model, were utilized to evaluate the relationship between IME and physical forces (SST, PAR, wind

magnitude, wind direction, wave power, wave direction, and MEI). Of the physical forces tested, SST and PAR were shown to have a significant relationship with IME.

IME presence and SST

A relationship between IME and SST was indicated by both Pearson's method and the GAM. The Pearson's method predicts the level of linear relationship and found there to be a mild positive relationship; when SST increased IME increased (r-value 0.15). The GAM indicated that the overall trend was when SST increased IME increased, although the relationship was more complicated.

Several studies have found relationships between SST and chlorophyll-a (Dunstan et al. 2018, Uz et al. 2017, and Yo-Lat et al. 2010). In a 14-year global study of SST and chlorophyll-a Dunstan et al. (2018) found that relationships between SST and chlorophyll-a varied greatly in different locations. Increased SST was found with increased chlorophyll-a in areas near ENSO and Interdecadal Pacific Oscillation (IPO) activity. Increased SST was found with decreased chlorophyll-a in areas with increased stratification and a deeper thermocline. Dunstan et al. (2018) note that coastal areas have a more complex relationship between SST and chlorophyll-a and that relationships between the variables are dependent on location. Given this, while the positive relationship between IME and SST were confirmed in this study by two separate statistical tests, we note that this relationship is specific for Rangiroa Atoll.

Chlorophyll-a concentration 46 km offshore to the north of Tiputa Channel are likely influenced by global climate variations of ENSO. Research by Uz et al. (2017) identified patterns of high and low chlorophyll-a in the equatorial Pacific between 10° N and 10° S corresponding to La Niña (cooling event, high chlorophyll-a) and El Niño (warming event, low chlorophyll-a). Changes in the thermocline and upwelling intensity related to El Niño and La Niña, resulted in changes in chlorophyll-a (Uz et al. 2017). If open ocean chlorophyll-a is depressed during strong El Niño warming events in the waters far offshore of Rangiroa Atoll and Rangiroa Lagoon chlorophyll-a is less affected by El Niño, the result would be stronger IME during those events.

To check that IME is higher during warming events, it is necessary to look at the relationships between chlorophyll-a and SST at the two locations (near Tiputa Channel and 46 km offshore) separately (this section does not compare the IME to SST, rather it compares the absolute chlorophyll-a measurements and SST). First, the SST near Tiputa Channel and 46 km offshore to the north were tested with the Mann-Whitney U Test and found likely to be in the same distribution ($p > 0.05$). Since SST near Tiputa and 46 km offshore are likely of the same set, SST near Tiputa Channel was used to test the relationship with chlorophyll-a at each location. Using Pearson's pairwise correlation on SST and chlorophyll-a (not the IME) near Tiputa Channel (r-value -0.29) and 46 km offshore (r-value -0.37), both locations show a negative linear relationship (increased SST, decreased chlorophyll-a), however, the offshore location shows a stronger negative relationship. This stronger negative relationship for chlorophyll-a and SST offshore compared to near Tiputa Channel supports the positive relationship between SST and IME. Higher SST means lower chlorophyll-a offshore compared to near Tiputa Channel. Increased chlorophyll-a near shore as it is approached from the open ocean is IME.

Closer to Rangiroa, Yo-Lat et al. (2010) saw a similar pattern, increased SST and decreased chlorophyll-a (again, please keep in mind Yo-Lat was examining chlorophyll-a and not the IME). Yo-Lat et al. (2010) investigated satellite chlorophyll-a data between January 1996 and March 2000 in a study 124 km (14.1° S, 147.1° W) outside Rangiroa Atoll. Yo-Lat (2010) found a strong relationship between the timing of an El Niño warming event and satellite-derived chlorophyll. On a regional scale, 124 km outside the atoll, the El Niño event increased the SST and decreased the chlorophyll concentrations from September 1997 to March 1998. During strong La Niña events, which occurred between January and March 1996 as well as August 1998 and March 2000, SST was lowered and chlorophyll concentrations increased.

IME presence and PAR

Pearson's method and a General Additive Model (GAM) both showed a negative relationship between IME presence and PAR. High PAR and reduced chlorophyll-a biomass have been documented in other studies (Flombaum et al. 2013 and Jyothibabu et al. 2018). Photoinhibition was observed in *Prochlorococcus* with cell abundance reduced 31% off-peak for high levels of

PAR in a global study (Flowbaum et al. 2013). In a study of cloud cover in the Bay of Bengal by Jyothibabu et al. (2018), chlorophyll-a was found to increase at lower levels of PAR when compared to 100% light saturation. Jyothibabu et al. (2018) found that a high PAR resulted in low surface chlorophyll-a, but a deeper chlorophyll-a maximum of approximately 50 m. The MODIS sensor used in this study reports only the surface chlorophyll-a concentration, missing any deeper chlorophyll-a biomass. If the two study locations near Rangiroa react to PAR similarly to the Bay of Bengal, then it is possible that high PAR may reduce surface chlorophyll-a concentration while increasing chlorophyll-a concentrations deeper in the water column.

4.3. How Might Future Changes Affect the IME at Rangiroa?

Climate change is causing sea level rise, ocean warming and acidification (Goeldner-Gianella et al. 2019), and increasing the frequency and intensity of El Niño events (Wang et al. 2019), all of which will likely impact IME at Rangiroa.

Sea level rise threatens to change Rangiroa from a semi-enclosed atoll to a more open atoll, through both erosion and by submerging the southern fringing reef. Open atolls allow lagoon water to be flushed more quickly resulting in water with properties more similar to the surrounding ocean (Ferrier-Pagès and Furla 2001). Ocean warming and acidification will limit coral growth, prohibiting vertical atoll growth via coral as sea level rises (Goeldner-Gianella et al. 2019). In a study by Andréfouët et al. (2001) biomass and atoll residence time were found to be linearly related for large Tuamotu atolls, a more open atoll would have a reduced residence time, therefore a reduced biomass contribution to the coastal ocean and a reduction to the IME.

A warming ocean and atmosphere may alter wind and wave patterns. These changes may alter the atoll reef structure since different rim types were created under different wave forcing (Andréfouët et al. 2001). A change in rim type was observed at neighboring atoll Tikehau as the result of a southern swell in 1996 and two storms in 1998 and 2010 (Goeldner-Gianella et al. 2019, Duvat et al. 2017). A change in rim type would likely change the residence time of water in the lagoon. If the atoll becomes more open, the water becomes more oligotrophic like the ocean, which would, in theory, reduce the IME.

5. CONCLUSIONS

Tourism and pearl farming are the main sources of income in the Tuamotu Archipelago (Pagano et al. 2017), making Rangiroa's primary resource the biologically productive lagoon. A biological oasis, in the vast oligotrophic Pacific could not exist without increased nutrients supporting the phytoplankton base of the food web, therefore understanding IME is important to understanding the marine ecosystem and economy of the Tuamotu Archipelago. The exact mechanism for the increase in IME remains unknown, but it is clear that the lagoon is a source of increased resources for phytoplankton production compared to the oligotrophic ocean that surrounds it. *In situ* data shows the water flowing out the atoll on the flood tide is warmer, less saline, less dense and lower in transparency than water flowing into the atoll. The relatively lower transparency water indicates higher concentrations of particulates are being advected from the inner lagoon in Rangiroa to the coastal ocean. This particulate matter likely contains a mix of organic and inorganic matter, which can support phytoplankton growth.

This study sought to demonstrate the occurrence of IME at Rangiroa and its relationship to physical forces. *In situ* and satellite data were analyzed. There is evidence that IME occurs near Tiputa Channel, this is supported by the average 16% increase in chlorophyll-a found when near Tiputa Channel is compared to 46 km offshore over the 16-year record. Fuel for the IME is likely the particulate-rich advected water forced by tides and modulated by waves. IME is most likely to occur with higher mean SST and lower mean PAR.

REFERENCES

- Abbott, Martin Lee. 2017. "Using Statistics in the Social and Health Sciences with SPSS ® and Excel ® , First Edition." 332-347. Hoboken, New Jersey: John Wiley & Sons, Inc.
- Andréfouët, S., J. Pagès, and B. Tartinville. 2001. "Water renewal time for classification of atoll lagoons in the Tuamotu Archipelago (French Polynesia)." *Coral Reefs* 20 (4): 399-408.
- Andréfouët, S., M. Claereboudt, P. Matsakis, J. Pagès, and P. Dufour. 2001. "Typology of atoll rims in Tuamotu Archipelago (French Polynesia) at landscape scale using SPOT HRV images." *International Journal of Remote Sensing* 22 (6): 987-1004.
- Andréfouët, Serge, Fabrice Ardhuin, Pierre Queffeuilou, and Romain Le Gendre. 2012. "Island shadow effects and the wave climate of the Western Tuamotu Archipelago (French Polynesia) inferred from altimetry and numerical model data." *Marine Pollution Bulletin* 65 (10-12): 415-424.
- Biospherical Instruments Inc. 2007. "QSP-2200 QPC-2200 Analog Output Quantum Profiling Sensor User's Manual."
- Brewin, Robert J.W., Giorgio Dall'Olmo, Silvia Pardo, Virginie van Dongen-Vogels, and Emmanuel S. Boss. 2016. "Underway spectrophotometry along the Atlantic Meridional Transect reveals high performance in satellite chlorophyll retrievals." *Remote Sensing of Environment* (Elsevier Inc.) 183: 82-97.
- Caldeira, R. M.A., S Groom, P Miller, D Pilgrim, and N P Nezlin. 2002. "Sea-surface signatures of the island mass effect phenomena around Madeira Island, Northeast Atlantic." *Remote Sensing of Environment* 80 (2): 336-360.
- Callaghan, David P., Peter Nielsen, Nick Cartwright, Michael R. Gourlay, and Tom E. Baldock. 2006. "Atoll lagoon flushing forced by waves." *Coastal Engineering* 53 (8): 691-704.
- Charpy, Loïc. 1996. "Phytoplankton biomass and production in two tuamotu atoll lagoons (French polynesia)." *Marine Ecology Progress Series* 145 (1-3): 133-142.
- Charpy, Loïc, Martine Rodier, Jonathan Fournier, Marie José Langlade, and Nabila Gaertner-Mazouni. 2012. "Physical and chemical control of the phytoplankton of Ahe lagoon, French Polynesia." *Marine Pollution Bulletin* 65 (10-12): 471-477.
- Charpy, Loïc, Philippe Dufour, and Nicole Garcia. 1997. "Particulate organic matter in sixteen Tuamotu atoll lagoons (French Polynesia)." *MARINE ECOLOGY PROGRESS SERIES Mar Ecol Prog Ser* 151: 55-65.
- Charpy-Roubaud, C, L Charpy, and A W D Larkum. 2001. "Atmospheric dinitrogen fixation by benthic communities of Tikehau Lagoon (Tuamotu Archipelago, French Polynesia) and its contribution to benthic primary production." *Marine Biology* 139: 991-998.

- Charpy-Roubaud, C.J., L. Charpy, and J.L. Cremoux. 1990. "Nutrient budget of the lagoonal waters in an open central South Pacific atoll (Tikehau, Tuamotu, French Polynesia)." *Marine Biology* 107: 67-73.
- Chevalier, C., J. L. Devenon, M. Pagano, G. Rougier, J. Blanchot, and R. Arfi. 2017. "The atypical hydrodynamics of the Mayotte Lagoon (Indian Ocean): Effects on water age and potential impact on plankton productivity." *Estuarine, Coastal and Shelf Science* 196: 182-197.
- Dandonneau, Yves, and Loïc Charpy. 1985. "An empirical approach to the island mass effect in the south tropical Pacific based on sea surface chlorophyll concentrations." *Deep Sea Research Part A, Oceanographic Research Papers* 32 (6): 707-721.
- Delesalle, B, and A Sournia. 1991. "Residence time of water and phytoplankton biomass in coral reef lagoons." *Continental Shelf Research* 12 (178): 939-949.
- Doty, M., Oguri, M.S. 1956. "The Island Mass Effect." *ICES Journal of Marine Science* 33-37.
- Dunstan, Piers K., Scott D. Foster, Edward King, James Risbey, Terence J. O’Kane, Didier Monselesan, Alistair J. Hobday, Jason R. Hartog, and Peter A. Thompson. 2018. "Global patterns of change and variation in sea surface temperature and chlorophyll a." *Scientific Reports* (Nature Publishing Group) 8 (1): 14624.
- Duvat, Virginie K E, Bernard Salvat, and Camille Salmon. 2017. "Drivers of shoreline change in atoll reef islands of the Tuamotu Archipelago, French Polynesia." *Global and Planetary Changes* 158:134-154.
- Ferrier-Pagès, Christine, and Paola Furla. 2001. "Pico- and nanoplankton biomass and production in the two largest atoll lagoons of French Polynesia." *MARINE ECOLOGY PROGRESS SERIES Mar Ecol Prog Ser* 211: 63-76.
- Flombaum, Pedro, José L Gallegos, Rodolfo A Gordillo, José Rincón, Lina L Zabala, and Nianzhi Jiao. 2013. "Present and future global distributions of the marine Cyanobacteria *Prochlorococcus* and *Synechococcus*." 110 (24): 9824–9829.
- Goeldner-Gianella, Lydie, Delphine Grancher, Alexandre K. Magnan, Edouard de Belizal, and Virginie K.E. Duvat. 2019. "The perception of climate-related coastal risks and environmental changes on the Rangiroa and Tikehau atolls, French Polynesia: The role of sensitive and intellectual drivers." *Ocean and Coastal Management* (Elsevier Ltd) 172: 14-29.
- Goldberg, Walter M. 2016. "Atolls of the world: Revisiting the original checklist." *Atoll Research Bulletin* 2016 (610).
- Gove, Jamison M., Margaret A. McManus, Anna B. Neuheimer, Jeffrey J. Polovina, Jeffrey C. Drazen, Craig R. Smith, Mark A. Merrifield, et al. 2016. "Near-island biological hotspots in barren ocean basins." *Nature Communications* (Nature Publishing Group) 7: 1-8.

- Hamner, W. M., and I R Hauri. 1981. "Effects of island mass: Water flow and plankton pattern around a reef in the Great Barrier Reef lagoon, Australia1." *Limnology and Oceanography* 26 (6): 1084-1102.
- Jyothibabu, R., N. Arunpandi, L. Jagadeesan, C. Karnan, K. R. Lallu, and P. N. Vinayachandran. 2018. "Response of phytoplankton to heavy cloud cover and turbidity in the northern Bay of Bengal." *Scientific Reports* 8 (1): 11282.
- Kirk, J T O. 2011. "Light and Photosynthesis in Aquatic Ecosystems. 3rd ed." 265-268. Cambridge, UK ; New York: Cambridge University Press.
- Kruger, Jens. 2013. *Tiputa Channel*. SPC Applied Geoscience and Technology Division (SOPAC).
- Kumar, S, J Kruger, Z Begg, E Handerson, and M Alvis. 2013. "Multibeam Bathymetry Survey Rangiroa , French Polynesia."
- Leichter, James J., M. Dale Stokes, James L. Hench, Jan Witting, and Libe Washburn. 2012. "The island-scale internal wave climate of Moorea, French Polynesia." *Journal of Geophysical Research: Oceans* 117 (6): 1-16.
- Lo-Yat, Alain, Stephen D. Simpson, Mark Meekan, David Lecchini, Elodie Martinez, and René Galzin. 2011. "Extreme climatic events reduce ocean productivity and larval supply in a tropical reef ecosystem." *Global Change Biology* (John Wiley & Sons, Ltd (10.1111)) 17 (4): 1695-1702.
- Martinez, Elodie, and Keitapu Maamaatuaiahutapu. 2004. "Island mass effect in the Marquesas Islands: Time variation." *Geophys. Res. Lett* 31.
- Möhlenkamp, Paula, Charles Kaiaka Beebe, Margaret A. McManus, Angela Hi ilei Kawelo, Keli'iahonui Kotubetey, Mirielle Lopez-Guzman, Craig E. Nelson, and Rosanna Anolani Alegado. 2018. "Ku Hou Kuapa: Cultural restoration improves water budget and water quality dynamics in He'eia Fishpond." *Sustainability (Switzerland)* (MDPI AG) 11 (1).
- Moore, Timothy S., Janet W. Campbell, and Mark D. Dowell. 2009. "A class-based approach to characterizing and mapping the uncertainty of the MODIS ocean chlorophyll product." *Remote Sensing of Environment* 113 (11): 2424-2430.
- Pagès, J., and S. Andréfouët. 2001. "A reconnaissance approach for hydrology of atoll lagoons." *Coral Reefs* 20 (4): 409-414.
- R Core Team. 2019. "R: A language and environment for statistical computing. R Foundation for Statistical Computing." Vienna, Austria. <https://www.R-project.org/>.
- Rogers, Justin S., Stephen G. Monismith, Oliver B. Fringer, David A. Kowek, and Robert B. Dunbar. 2017. "A coupled wave-hydrodynamic model of an atoll with high friction: Mechanisms for flow, connectivity, and ecological implications." *Ocean Modelling* (Elsevier Ltd) 110: 66-82.

- Sauzède, Raphaëlle, Elodie Martinez, Orens Pasqueron de Fommervault, Antoine Poteau, Alexandre Mignot, Christophe Maes, Hervé Claustre, et al. 2018. "Seasonal dynamics and disturbance of phytoplankton biomass in the wake of Tahiti as observed by Biogeochemical-Argo floats." *Biogeosciences Discussions* 1-35.
- Spall, Michael A, and Joseph Pedlosky. 2013. "Interaction of Ekman Layers and Islands." *Journal of Physical Oceanography* 43 (5): 1028-1041.
- Spiegel, Murray R, and Larry J Stephens. 2011. "Schaums Outlines Statistics." 348-350. New York: McGraw-Hill.
- Uz, Stephanie Schollaert, Antonio J. Busalacchib, Thomas M. Smith, Michael N. Evans, Christopher W. Brown, and Eric C. Hackert. 2017. "Interannual and decadal variability in tropical Pacific chlorophyll from a statistical reconstruction: 1958-2008." *Journal of Climate* (American Meteorological Society) 30 (18): 7293-7315.
- Wang, Bin, Xiao Luo, Young Min Yang, Weiyi Sun, Mark A. Cane, Wenju Cai, Sang Wook Yeh, and Jian Liu. 2019. "Historical change of El Niño properties sheds light on future changes of extreme El Niño." *Proceedings of the National Academy of Sciences of the United States of America* (National Academy of Sciences) 116 (45): 22512-22517.
- Woodroffe, Colin D, and Naomi Biribo. 2011. "Atolls." In *Encyclopedia of Modern Coral Reefs: Structure, Form, and Process*, by Colin D Woodroffe and Naomi Biribo, 1-21.